博士論文

Fermi-surface effect on the Fulde-Ferrell-Larkin-Ovchinnikov
state in quasi-one-dimensional superconductors
（準一次元超伝導体におけるＦＦＬＯ状態に対するフェルミ面効果）

宮脇　信実

広島大学大学院先端物質科学研究科

2014年3月

Contents

1. INTRODUCTION

The Fulde–Ferrell–Larkin–Ovchinnikov (FFLO) state [1, 2] has been investigated both experimentally and theoretically as reviewd in some articles [3–5]. Following the theoretical prediction of Fulde and Ferrell [1] and Larkin and Ovchinnikov [2], there has been no convincing experimental evidence of the FFLO state, but recently its occurrence has been suggested in strongly Pauli-limited clean type-II superconductors.

At the present, the candidate compounds are the heavy-fermion superconductor $CeCoIn_5$ [4] and the quasi-low-dimensional organic superconductors [5–40], such as κ–(BEDT-TTF)$_2$Cu(NCS)$_2$ [12–15], λ-(BETS)$_2$FeCl$_4$ [18–20], λ-(BETS)$_2$GaCl$_4$ [21], and (TMTSF)$_2$ClO$_4$ [24–26, 28–40]. Interestingly, all of these compounds are quasi-low-dimensional with respect to the conduction electron states.

The quasi-low-dimensionality stabilizes the FFLO state for two reasons. First, the orbital pair-breaking effect is suppressed by orienting the magnetic field in the direction parallel to the most conductive layer. Particularly in organics, the magnetic field must be precisely aligned for the occurrence of the FFLO state [41]. Second, the highly anisotropic structure of the Fermi surfaces in quasi-low-dimensional systems stabilizes the FFLO state. The center-of-mass momentum $\boldsymbol{q}$ of the Cooper pairs is finite in the FFLO state, and it gives rise to the spatial modulation of the order parameter characteristic of the FFLO state. Since realistic materials have anisotropic Fermi surfaces, there exists the optimum direction of $\boldsymbol{q}$ for which the upper critical field is maximum. When $\boldsymbol{q}$ is oriented in the optimum direction, the FFLO state is stabilzed most. We term this the Fermi-surface effect from now on. In anisotropic superconductors, the structure of the gap function significantly affects the Fermi-surface effect [9, 10].

Among the above candidate compounds, the quasi-one-dimensional organic superconductor (TMTSF)$_2$ClO$_4$ [25, 26, 28–33] has attracted current interest. The electron energy dispersions of the organic superconductors (TMTSF)$_2$X (X = ClO$_4$, PF$_6$ etc.) can be expressed by the Q1D tight-binding model ($t_a > t_b \gg t_c$). In (TMTSF)$_2$PF$_6$, H_{c2} exceeds the Pauli paramagnetic (Chandrasekhar-Clogston) limit [42] [22]. However, this compound is likely to be spin triplet super-

conductivity [23]. In $(TMTSF)_2ClO_4$, H_{c2} exceeds the Pauli paramagnetic limit H_P for both $\boldsymbol{a}$- and $\boldsymbol{b}'$-axis [24–26], and a new principal axis different from the crystal axis emerges above the Pauli paramagnetic limit, which may be related to occurrence of the FFLO state [25, 26]. This compound is likely to be a spin singlet superconductivity with line nodes (d-wave state) [27]. In addition, an upturn of the temperature dependence of the upper critical field $H_{c2}(T)$ at low temperature is consistent with the FFLO $H_{c2}(T)$ in quasi-low-dimensional systems [8–10, 20, 43, 44].

For this compound, many theoretical studies have been proposed with respect to the FFLO state. Recently, Lebed et al. have calculated the upper critical fields in $\boldsymbol{a}$- and $\boldsymbol{b}'$-axis, taking into account both the Pauli paramagnetic and orbital pair-breaking effect [28, 31]. The resultant values are quantitatively consistent with the experimental data. Especially, for the magnetic field in the direction of $\boldsymbol{b}'$-axis, the field-induced dimensional-crossover [7, 45] leads to a hidden reentrant and FFLO state to coexist. On the other hand, Croitoru et al. have examined angular dependence of the upper critical field in systems with elliptic Fermi-surfaces [29]. It has been shown that the transition temperature is maximal for the magnetic field oriented perpendicular to $\boldsymbol{q}$. Lebed et al. [31] and Fuseya et al. [33] have investigated this compound, but they also have assumed simplified Fermi-surfaces. However, in such systems, the nesting effect of the Q1D Fermi-surface is not taken into account correctly.

In spite of the these theoretical studies, the limits of the pure FFLO state have not been reported in Q1D systems. In this thesis, we investigate the nesting effect taking into account Q1D Fermi-surface structure in more detail [40]. A novel dimensional crossover, which is induced by temperature effect is reported. In addition, for the warped Fermi surface, since the direction of the optimum $\boldsymbol{q}$ is nontrivial [9, 10], we decide the directions of $\boldsymbol{q}$ where $H_{c2}(T)$ is maximal.

In $(TMTSF)_2ClO_4$, there is no consensus of the value of hopping energies t_b/t_a. Yonezawa et al. and Lebed have estimated the values to be about 0.26 and 0.1 by the Ginzburg-Landau slopes [26, 34]. The value determined by Huckel methods [35] and first principles methods [36] has been estimated to be about 0.2. In Q1D systems, the values of t_b/t_a assumed in previous studies are summarized in Table I. We show

the t_b/t_a dependence of H_{c2} in detail.

TABLE I: The approximate values of t_b/t_a assumed in previous studies of Q1D systems.

t_b/t_a	0.07	0.1	0.2	0.26
references	[37]	[6, 7, 28, 30, 31, 34, 38, 39]	[32, 35, 36]	[26]

The paper is organized as follows. In Sect. 2, fundamental properties of the FFLO state is reviewed. In Sect. 3, the nesting effect of the FFLO state is discussed. Sect. 4 is devoted to the purpose of this study. In Sect. 5, the equations for T_c, H_{c2} and H_P are formulated. In Sect. 6, numerical results are presented. In Sect. 7, we summarize the results and discuss. We use the units where $\hbar = 1$ and $k_B = 1$ throughout.

2.   FFLO STATE

In this section, we review the fundamental properties of the FFLO state. The FFLO state is the superconducting state in which the Cooper pairs have a finite center-of-mass momentum $\boldsymbol{q}$ as shown in Fig. 1 (b) because of the spin polarization energy, in contrast to the BCS state in which the center-of-mass momentum of the Cooper pairs is zero as shown in Fig. 1 (a). In the absence of the magnetic field, the latter state is more favorable than the fomer state, because the condensation energy of the former state is larger than the latter state. However, when sufficiently strong magnetic field is applied to type-II superconductors, the BCS state becomes unstable because of the spin polarization energy. The critical magnetic field is estimated by the condition that the loss in the spin polarization energy $(1/2)N\chi H^2$ reaches the superconducting condensation energy $(1/2)NN(0)\Delta_0^2$. The limiting field by this pair-breaking effect is called the Pauli paramagnetic (Chandrasekhar-Clogston) limit $H_{\mathrm{P}}(T)$ [42], which is nothing but the upper critical field of the superconductivity when the orbital pair-breaking effect is not considered. The transition between the normal state and the BCS state at this field is the first order. It is known that the Pauli paramagnetic limit for s-wave $\mu_e H_{\mathrm{P}}(0)/\Delta_0$ is equal to $1/\sqrt{2}$.
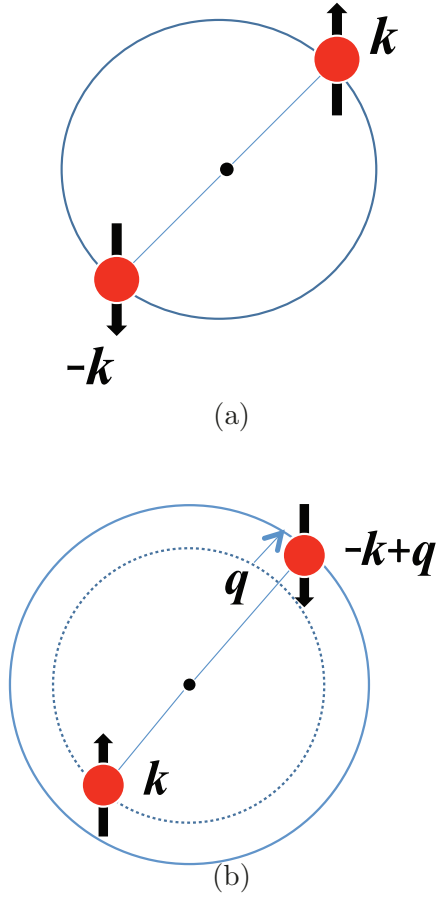
FIG. 1: Schematic figures of the pairing states (a) in the BCS state ($\boldsymbol{k}\uparrow$, $-\boldsymbol{k}\downarrow$), and (b) in the FFLO state ($\boldsymbol{k}\uparrow$, $-\boldsymbol{k}+\boldsymbol{q}\downarrow$) when the Fermi surfaces split by the Zeeman energy. In the figure (b), the solid and dotted curves present the Fermi surfaces of spin-down electrons and spin-up electrons, respectively.

The superconductivity is broken by the magnetic fields because of the Pauli paramagnetic and orbital pair-breaking effects. In the present paper, we examine the case that the orbital pair-breaking effect is weak. In the FFLO state, the spin polarization energy is larger than that in the BCS state, while the superconducting condensation energy is smaller because of the kinetic energy of the Cooper pairs. When the Fermi surfaces split because of the Zeeman energy, the superconductivity can occur by pairing of two electrons with $(\boldsymbol{k},\uparrow)$ and $(-\boldsymbol{k}+\boldsymbol{q},\downarrow)$.

Figure 2 displays the schematic phase diagram when the FFLO state occurs. In

the presence of the orbital pair-breaking effect, the transition at the upper critical field $H_{c2}(T)$ is of second-order. On the other hand, in the absence of the orbital pair-breaking effect, the second-order transition field between the BCS and normal states is lower than the first-order transition field of the Pauli paramagnetic limit H_P of the BCS state. This implies that the second-order transition line is fictitious or metastable line. For the FFLO state to occur, the second-order transition field to the FFLO state must exceed H_P. In the case that the FFLO state enhances the upper critical field of the superconductivity, the transition field between the FFLO and BCS states is lower than H_P, because in such a case the free energy of the FFLO state is lower than that of the normal state. In the absence of the orbital pair-breaking effect, the FFLO state occurs below the tricritical temperature $T^* \approx 0.56T_c$, which does not depend on the dimensionality of the system, although it is lowered by the orbital effect.
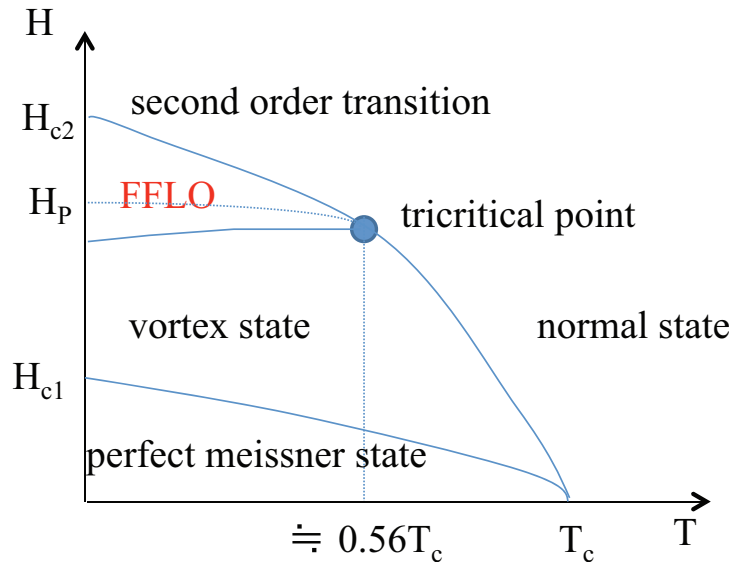
FIG. 2: Phase diagram of the FFLO state. The dotted curve shows the first-order transition from the BCS state to the normal state.

In three dimensional (3D) isotropic systems, the FFLO upper critial field is slightly higher than $H_P(T)$, and the area of the FFLO state in the phase diagram

is narrow. Considering the orbital pair-breaking effect and so on, the FFLO state would not occur in such systems. On the other hand, in quasi-two-dimensional (Q2D) isotropic systems, it has been found that the nesting effect widen the area of the FFLO state. This indicates the possibility of the realization of the FFLO state in quasi-low-dimensional systems [8]. The behavior of the upper critical field at $T = 0$ can be classified depending on the nesting condition. For the 3D isotropic systems, the nesting condition is "crossing along a line". This type of nesting results in $dH_{c2}(0)/dT = 0$. Whereas, in the Q2D systems, the nesting condition is "touching on a line", and the $H_{c2}(T)$ exhibits a upturn near $T = 0$. This results in $dH_{c2}(T)/dT > 0$. The relation between the nesting conditions and the behavior of the upper critical fields is discussed in the next section.

Next, we discuss the spacial oscillation of the order parameter in the FFLO state. The order parameter of the superconductivity is generalized to include the FFLO state as

$$\Delta_{\boldsymbol{q}}^*(\boldsymbol{k}) = \langle a_{-\boldsymbol{k}+\boldsymbol{q}/2\downarrow}^\dagger a_{\boldsymbol{k}+\boldsymbol{q}/2\uparrow}^\dagger \rangle, \tag{2.1}$$

where $\boldsymbol{q}$ and $\boldsymbol{k}$ are the center-of-mass and the relative momenta, respectively. In the coordinate representation, the order parameter is expressed as

$$\Delta^*(\boldsymbol{r}, \boldsymbol{r}') = \langle \psi_\downarrow^\dagger(\boldsymbol{r}) \psi_\uparrow^\dagger(\boldsymbol{r}') \rangle. \tag{2.2}$$

By the Fourier transformation for $\psi_\sigma^\dagger(\boldsymbol{r})$, Eq. (2.2) is written as

$$\Delta^*(\boldsymbol{r}, \boldsymbol{r}') = \frac{1}{N} \sum_{\boldsymbol{p}} \sum_{\boldsymbol{p}'} e^{-i(\boldsymbol{p}\cdot\boldsymbol{r}+\boldsymbol{p}'\cdot\boldsymbol{r}')} \langle a_{\boldsymbol{p}\downarrow}^\dagger a_{\boldsymbol{p}'\uparrow}^\dagger \rangle. \tag{2.3}$$

Then, the order parameter is expressed in terms of the center-of-mass coordinate $\boldsymbol{R}$ and the relative coordinate $\boldsymbol{\rho}$ as

$$\Delta^*(\boldsymbol{R}, \boldsymbol{\rho}) = \frac{1}{N} \sum_{\boldsymbol{q}} \sum_{\boldsymbol{k}} e^{-i(\boldsymbol{q}\cdot\boldsymbol{R}+\boldsymbol{k}\cdot\boldsymbol{\rho})} \langle a_{\boldsymbol{k}+\boldsymbol{q}/2\downarrow}^\dagger a_{-\boldsymbol{k}+\boldsymbol{q}/2\uparrow}^\dagger \rangle. \tag{2.4}$$

By the Fourier transformation with respect to $\boldsymbol{\rho}$, Eq. (2.4) is rewritten as

$$\Delta^*(\boldsymbol{R}, \boldsymbol{k}) = \sum_{\boldsymbol{q}} e^{-i\boldsymbol{q}\cdot\boldsymbol{R}} \langle a_{-\boldsymbol{k}+\boldsymbol{q}/2\downarrow}^\dagger a_{\boldsymbol{k}+\boldsymbol{q}/2\uparrow}^\dagger \rangle = \sum_{\boldsymbol{q}} e^{-i\boldsymbol{q}\cdot\boldsymbol{R}} \Delta_{\boldsymbol{q}}^*(\boldsymbol{k}). \tag{2.5}$$

Thus, the order parameter has the spatial oscillation factors $e^{-i\boldsymbol{q}\cdot\boldsymbol{R}}$. Hence, the nonzero center-of-mass momenta $\boldsymbol{q}$'s give rise to the spacial oscillation of the order parameter with respect to the center-of-mass coordinate $\boldsymbol{R}$.

Fulde and Ferrell examined the state in which $\Delta_{\boldsymbol{q}}(\boldsymbol{k}) \neq 0$ for a single $\boldsymbol{q}$ [1]. In this state, the order parameter in the real space oscillate in the form

$$\Delta(\boldsymbol{R}, \boldsymbol{k}) = \Delta_1(\boldsymbol{k})e^{i\boldsymbol{q}\cdot\boldsymbol{R}}. \tag{2.6}$$

Larkin and Ovchinnikov [2] proved that for the 3D isotropic systems the order parameter expressed by the linear combinations of $e^{i\boldsymbol{q}\cdot\boldsymbol{R}}$ and $e^{-i\boldsymbol{q}\cdot\boldsymbol{R}}$

$$\Delta(\boldsymbol{R}) = \Delta_1(e^{i\boldsymbol{q}\cdot\boldsymbol{R}} + e^{-i\boldsymbol{q}\cdot\boldsymbol{R}}) = 2\Delta_1 \cos(\boldsymbol{q}\cdot\boldsymbol{R}), \tag{2.7}$$

is more stable than the order parameter Eq. (2.6). Depending on the literature, the order parameters Eq. (2.6) and Eq. (2.7) are called the FF state and the LO state, respectively. For the isotropic 2D systems, it has been proved that the order parameters expressed by generalized linear combinations are more stable than the FF state and LO state [46]. In general, the order parameter is written as

$$\Delta(\boldsymbol{R}) = \sum_{m=1}^{M} \Delta_m e^{i\boldsymbol{q}_m\cdot\boldsymbol{R}}. \tag{2.8}$$

These states have the same upper critical field within the second order transition. When the system is isotropic, the degeneracy of $\boldsymbol{q}$ is infinite, but if we assume the periodic structure of the order parameter in the real space, the value of M can be equal to 1, 2, 3, 4, and 6. When the Fermi surface has anisotropic structure, the number of the equivalent $\boldsymbol{q}$ is related to the symmetry of the Fermi surface. In the Q1D systems near the upper critical fields, it is expected that $M = 2$ if $\boldsymbol{q} \parallel \boldsymbol{a}$ or $\boldsymbol{b}$, while $M = 4$ otherwise.

3.　NESTING EFFECT

In this section, the concept of Fermi-surface "nesting" for the FFLO state has been introduced [8–10] in order to investigate the Fermi-surface effect, which is analogous to those for the charge-density-wave (CDW) and spin-density-wave (SDW). Because the FFLO state consist of the Cooper pairs of electrons with $(\boldsymbol{k}, \uparrow)$ and $(-\boldsymbol{k}+\boldsymbol{q}, \downarrow)$, the stability of the state is closely related to the extent of the overlap of the Fermi surfaces of spin-up and spin-down electrons. Figure 3 is schematic figure of the nesting condition. The former Fermi surface is inverted and shifted by $\boldsymbol{q}$, which is expressed as $\boldsymbol{k} \rightarrow -\boldsymbol{k}+\boldsymbol{q}$.
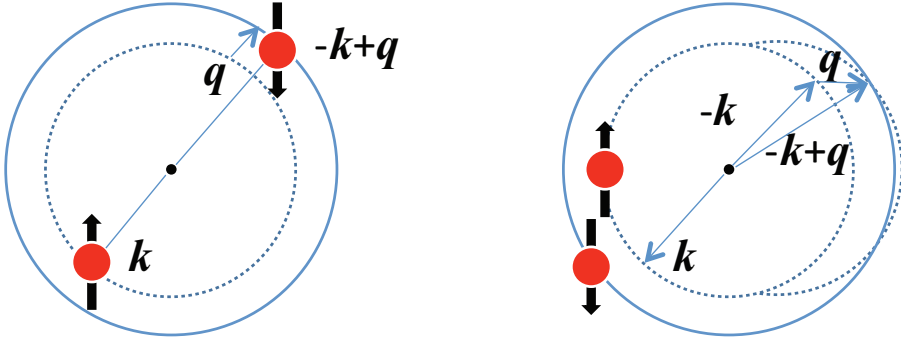
FIG. 3: Nesting condition of FFLO state. The solid and dotted curves present the Fermi surfaces of spin-down electrons and spin-up electrons, respectively.

In the one dimensional (1D) systems, the upper critical field $H_{c2}(T)$ diverges at $T \rightarrow 0$ [47–49]. Such divergence is due to perfect nesting, which means that the overlap occurs in a finite area on the Fermi surface, classified as type (a) in Table II. However, for realistic interaction strengths, such 1D systems should undergo the nesting instabilities to CDW or SDW. Therefore, the best candidate is a quasi-two-dimensional (Q2D) system, in which the CDW and SDW transitions are suppressed. In such systems, the Fermi surfaces touch on one or more lines by the transformation $\boldsymbol{k} \rightarrow -\boldsymbol{k}+\boldsymbol{q}$ of the spin-down Fermi surface[8–10]. The nesting condition of Q2D isotropic systems is shown in figure 4. This type of nesting results in $H'_{c2}(0) \neq 0$ and $H_{c2}(0) < \infty$ and the upturn of $H_{c2}(T)$ at low temperatures, classified as type (b)

in Table II, where $H'_{c2}(T) \equiv \mathrm{d}H_{c2}/\mathrm{d}T$. In Q2D systems, the nesting enhances the FFLO state, but at the same time, it suppresses the CDW and SDW instabilities [8].
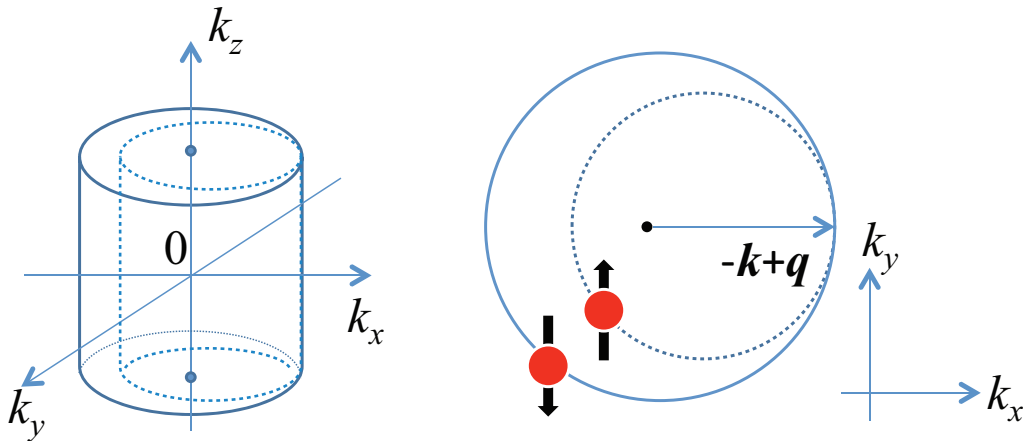
FIG. 4: Nesting condition in Q2D systems. See the caption of Fig. 3 for the meaning of the difference lines.

Here, we should note that the Q2D systems in this context include Q1D systems in which the interchain hopping energy t_b is large enough to suppress the CDW and SDW transitions. Although $(\mathrm{TMTSF})_2 X$ is called Q1D, it should be classified as Q2D regarding the nesting effect for the FFLO state.

On the other hand, in isotropic systems having spherical Fermi surfaces, the upper critical field of the FFLO state is only slightly higher than the Pauli paramagnetic limit of the BCS state as mentioned above. In such systems, $|\boldsymbol{q}|$ becomes larger than $2h/v_\mathrm{F}$, which is the separation between the Fermi surfaces of the spin-up and spin-down electrons, since "crossing along a line" is a better nesting condition than "touching at a point". Figure 5 displays the nesting condition of 3D isotropic systems. Such a nesting condition leads to $H'_{c2}(0) = 0$, which is classified as type (c) in Table II.

11
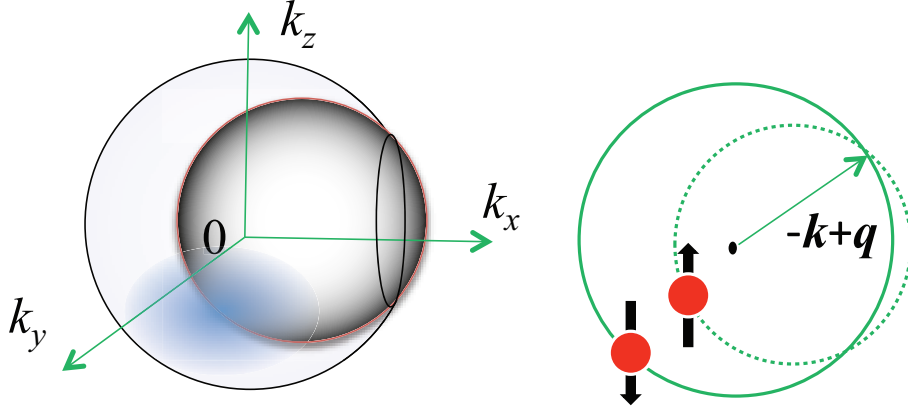
FIG. 5: Nesting condition in isotropic 3D systems. See the caption of Fig. 3 for the meaning of the difference lines.

Figure 6 shows the relation between the upper critical fields with the dimensions of systems. In Table II, the low-temperature behaviors of $H_{c2}(T)$ are summarized. The Q1D compounds, such as $(\mathrm{TMTSF})_2 X$ should be classified as type (b), because the Fermi surfaces are sufficiently warped. However, the behavior of the upper critical field is more complicated at high temperatures, because of the shape of the Fermi surface, the density of states, the gap anisotropy, and so on. In fact, hybrid behaviors of types (a) to (c) occur in the intermediate temperature region $T \lesssim T^*$, depending on t_b/t_a and φ, where φ is the angle between $\boldsymbol{q}$ and the crystal $\boldsymbol{a}$-axis.
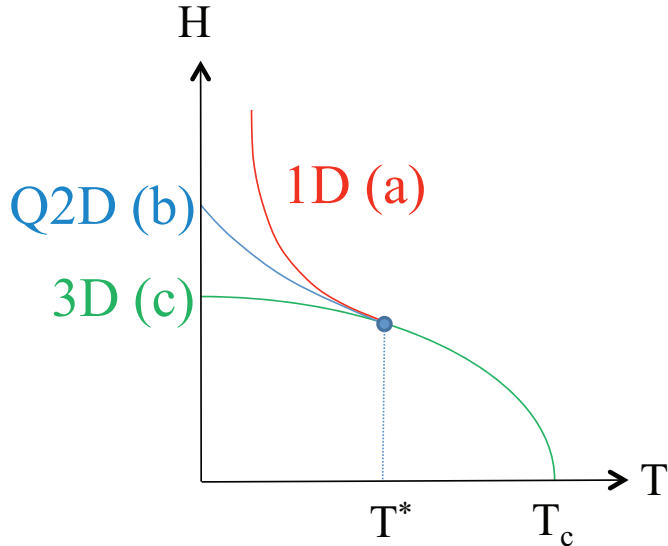
FIG. 6: Upper critical fields for 1D, Q2D and 3D systems.

TABLE II: Nesting conditions and low-temperature behaviors of $H_{c2}(T)$ (from Ref. [40]).

type	nesting	$H_{c2}(0)$	$H'_{c2}(0)$	$H''_{c2}(T)$
(a)	touch on a surface	infinite	N/A	positive
(b)	touch on a line	finite	negative	positive
(c)	crossing along a line	finite	zero	negative

Let us consider the model that has Q1D energy dispersion

$$\xi_\sigma(\boldsymbol{k}, h) = -2t_a \cos(\boldsymbol{k} \cdot \boldsymbol{a}) - 2t_b \cos(\boldsymbol{k} \cdot \boldsymbol{b}) - h\sigma - \mu, \qquad (3.1)$$

where μ_e and μ are the magnitudes of the electron magnetic moment and chemical potential, respectively. We have defined $h = \mu_e|\boldsymbol{H}|$. In Eq. (3.1), we have assumed that $t_a > t_b \gg t_c$, and omitted the interplane hopping energy t_c for simplicity. However, it is supposed that t_c is large enough to stabilize the superconducting

13

long-range order, and to justify the mean-field approximation, but that it is small enough to omit in the mean-field self-consistent equations. Introducing reciprocal lattice vectors $\bar{\boldsymbol{a}}$, $\bar{\boldsymbol{b}}$, and $\bar{\boldsymbol{c}}$, and the momentum components k_x, k_y, and k_z via $\boldsymbol{k} = k_x \bar{\boldsymbol{a}} + k_y \bar{\boldsymbol{b}} + k_z \bar{\boldsymbol{c}}$, we obtain

$$\xi_\sigma(\boldsymbol{k}, h) = \xi_{\boldsymbol{k}} - h\sigma, \tag{3.2}$$

with

$$\xi_{\boldsymbol{k}} = -2t_a \cos(k_x) - 2t_b \cos(k_y) - \mu. \tag{3.3}$$

For simplicity of notation, we have redefined k_x and k_y so that they include the lattice constants a and b, respectively, which is equivalent to formally taking the length unit so that $a = b = 1$.

To study the nesting condition, let us define the energy difference

$$\Delta\epsilon(k_y, \boldsymbol{q}, h) \equiv \left[\xi_\uparrow(\boldsymbol{k}, h) - \xi_\downarrow(-\boldsymbol{k} + \boldsymbol{q}, h) \right]_{k_x = k_{\mathrm{F}x}^\uparrow(k_y)}, \tag{3.4}$$

with $k_{\mathrm{F}x}^\sigma(k_y)$ denoting a positive function that satisfies $\xi_\sigma(k_{\mathrm{F}x}^\sigma(k_y), k_y, h) = 0$. On the Fermi surface, define $\Delta k_{\mathrm{F}x}(k_y, \boldsymbol{q}) \equiv k_{\mathrm{F}x}^\downarrow(k_y) - [k_{\mathrm{F}x}^\uparrow(k_y - q_y) + q_x]$. For the vector $\boldsymbol{q}$ that satisfies $\Delta k_{\mathrm{F}x}(k_y, \boldsymbol{q}) = 0$, the energy difference $\Delta\epsilon(k_y, \boldsymbol{q}, h)$ is zero. If there exists a constant vector $\boldsymbol{q}$ such that $\Delta k_{\mathrm{F}x}(k_y, \boldsymbol{q}, h) = 0$ over a finite range of k_y values, perfect nesting occurs. In that case, $H_{c2}(T)$ diverges as $T \to 0$, as in case (a). However, such a constant vector $\boldsymbol{q}$ does not exist when $t_b \neq 0$.

The nesting condition is not correctly treated by the linearized energy dispersion relation

$$\xi_\sigma^{(\pm)}(\boldsymbol{k}, h) \approx \bar{v}_{\mathrm{F}} \left(k_x \pm p_{\mathrm{F}}(k_y, k_z) \right) + \epsilon_\perp(k_y, k_z) - h\sigma - \mu, \tag{3.5}$$

with a constant Fermi velocity $\bar{v}_{\mathrm{F}}$, as used by many previous authors, and $+(-)$ stands for the right (left) sheet of the Fermi surface. In this model, the displacement of the Fermi surfaces of spin-up and spin-down electrons due to the Zeeman energy $2h$ is compensated by a constant shift $\boldsymbol{q} = (2h/\bar{v}_{\mathrm{F}}, 0, 0)$ independent of (k_y, k_z). Therefore, this model exhibits the perfect nesting condition in the FFLO state. However, in realistic Q1D systems, the Fermi velocity v_{F} depends on k_y with a variation from $\bar{v}_{\mathrm{F}}$ of the order of $t_b \bar{v}_{\mathrm{F}}/t_a$, which is small but non-negligible. The variation of v_{F} causes a mismatch of the Fermi surfaces which significantly change the behavior of $H_{c2}(T)$ at low temperatures.

Equation (3.2) gives the magnitude of the Fermi velocity along the most conducting chain as $v_{\mathrm{F}} = 2t_a \sin(k_{\mathrm{F}x})$ in unit of $a/\hbar$, where $k_{\mathrm{F}x}$ denotes the Fermi momentum in the chain direction. For quarter-filled bands in the organics, since $k_{\mathrm{F}x} \sim \pi/4$, $v_{\mathrm{F}} \approx \sqrt{2}t_a \equiv \bar{v}_{\mathrm{F}}$ is obtained. The energy difference $\Delta\epsilon(k_y, \boldsymbol{q}, h)$ owing to $\Delta v_{\mathrm{F}} \equiv v_{\mathrm{F}} - \bar{v}_{\mathrm{F}}$ is estimated to be $\Delta v_{\mathrm{F}}q \lesssim t_b v_{\mathrm{F}}q/t_a \sim t_b T_{\mathrm{c}}^{(0)}/t_a$, since $v_{\mathrm{F}}q \sim h \sim T_{\mathrm{c}}^{(0)}$, using a value of $\boldsymbol{q}$ that makes the Fermi surfaces touch on a line at a point in the (k_x, k_y) plane, where $T_{\mathrm{c}}^{(0)}$ denotes the zero-field transition temperature. Therefore, the crossover temperature T_0 between the perfect and imperfect nesting conditions is proportional to $t_b T_{\mathrm{c}}^{(0)}/t_a$. The constant of proportionality can be small, because even if only a small portion of the Fermi surfaces touch on a surface, H_{c2} diverges in the limit $T \to 0$.

At higher temperatures $T^* \gtrsim T \gtrsim T_0$, one can neglect $\Delta\epsilon$ in comparison to the thermal energy $k_{\mathrm{B}}T$. Therefore, the upper critical field is not significantly affected by the small mismatch in the Fermi surfaces $\Delta k_{\mathrm{F}x}$ because of the temperature effect. Hence, the system behaves like a 1D system, in which the Fermi-surface nesting for the FFLO state is perfect. However, at low temperatures, $T \lesssim T_0$, the variation Δv_{F} due to the warp in the Fermi surface can be substantial. For $T \sim T_0$, the system begins to lose its 1D character, and when $T \ll T_0$ the two-dimensional (2D) character of the system is recovered. Hence, when the interchain hopping energy t_b is small enough that $T^* \gtrsim T_0 \propto t_b T_{\mathrm{c}}/t_a$ is satisfied, a dimensional crossover between one and two dimensions can take place [50]. In the section 6, it is proved by numerical calculations that such a crossover actually occurs.

4.   PURPOSE OF THIS STUDY

We analyze the pure FFLO state in Q1D systems for s- and d-wave pairings. It was suggested that the FFLO state occurs in a organic superconductor $(TMTSF)_2ClO_4$ [25, 26]. In $(TMTSF)_2ClO_4$, the line nodes are likely to exist, because the NMR measurements indicate that $1/T_1 \propto T^3$ [27]. Hence, in particular, we focus on the nodal d-wave pairings.

Although previous theoretical studies for the FFLO state are consistent with the experimental data, the Fermi-surface effect was not treated correctly. In the Q1D systems, t_b/t_a is large enough to suppress the CDW and SDW transitions. Therefore, the Q1D system is classified as Q2D with respect to the for the nesting effect of the FFLO state. Many previous authors assumed that the Fermi velocity v_F is constant [31, 33]. This situation implies the perfect nesting like 1D systems. We take into account the Q1D dispersion correctly, and predict a dimensional crossover between one and two dimensions. This crossover is induced by the temperature effect, which will be proved by numerical calculations in Sect. 3.

We will show H_{c2} for various ratios t_b/t_a. In $(TMTSF)_2ClO_4$, although the value of t_b/t_a has been estimated by some theoretical and experimental studies, a consensus on the ratio t_b/t_a has not been obtained. When t_b/t_a increases, since the warp in the Fermi surface increases, the system exhibits the 2D character. In that case, the effect to the dimensional crossover will be investigated.

The upper critical fields will be obtained for various directions of $\boldsymbol{q}$. Many previous authors assumed that the direction of $\boldsymbol{q}$ is oriented to a most conductive chain direction, where $\boldsymbol{q}$ is shortest. One may think that H_{c2} is maximum in the direction in which $\boldsymbol{q}$ is shortest, because the spacial oscillation in the order parameter $\Delta(\boldsymbol{r})$ is minimal. However, in the warp Fermi surface for the square lattice tight binding model, the optimum direction of $\boldsymbol{q}$ is nontrivial [10, 11]. In addition, for large angles between $\boldsymbol{q}$ and $\boldsymbol{a}$, the nesting condition has not been examined. We will clarify the relation between the nesting condition and the direction of $\boldsymbol{q}$ for both s- and d-wave pairings.

In this study, we will formulate the equations for T_c and H_{c2}, and temperature dependence upper critical fields are evaluated by the numerical calculations. The main

goals of this research are as follows: (1) A novel dimensional crossover predicted by nesting effect is verified numerically. (2) The upper critical fields $H_{c2}(T)$ for various ratios t_b/t_a are exhibited. (3) The upper critical fields for the various directions of $\boldsymbol{q}$ are shown. (4) We compare the theoretical results with the experimental data.

5. FORMULATION

In this section, the previous theory for the square lattice tight-binding model is extended to the present Q1D tight-binding model [10, 11]. In the following subsections, we formulate the equations for T_c, H_{c2} and H_P.

Considering the organic conductors, we assume quarter-filled band. We examine the Hamiltonian

$$H = \sum_{\boldsymbol{k}\sigma} \xi_\sigma(\boldsymbol{k}, h) a_{\boldsymbol{k}\sigma}^\dagger a_{\boldsymbol{k}\sigma} - \frac{1}{N} \sum_{\boldsymbol{q}} \sum_{\boldsymbol{k},\boldsymbol{k}'} V(\boldsymbol{k}, \boldsymbol{k}') a_{\boldsymbol{k}+\boldsymbol{q}/2\uparrow}^\dagger a_{-\boldsymbol{k}+\boldsymbol{q}/2\downarrow}^\dagger a_{-\boldsymbol{k}'+\boldsymbol{q}/2\downarrow} a_{\boldsymbol{k}'+\boldsymbol{q}/2\uparrow},$$

(5.1)

with the band dispersion of the Q1D tight-binding model (3.4), and the pairing interaction

$$V(\boldsymbol{k}, \boldsymbol{k}') = V_\alpha \gamma_\alpha(\boldsymbol{k}) \gamma_\alpha(\boldsymbol{k}'),$$

(5.2)

where N and V_α are the site number and the coupling constant of the α component of the pairing interactions. α is the symmetry index of the gap function. We examine s- and d-wave pairing, defining

$$\begin{cases} \gamma_s(k_y) = 1 \\ \gamma_d(k_y) = \sqrt{2}\cos k_y. \end{cases}$$

(5.3)

When $\boldsymbol{q} = 0$, the Hamiltonian is reduced to the conventional BCS Hamiltonian. We derive the gap equation following the same procedure as the BCS theory.

5.1. FFLO upper critical field at finite temperatures

We adopt the mean field approximation extended to the FFLO state as

$$H_{\mathrm{MF}} = \sum_{\boldsymbol{k}\sigma} \xi_\sigma(\boldsymbol{k}, h) a^\dagger_{\boldsymbol{k}\sigma} a_{\boldsymbol{k}\sigma} + \sum_{\boldsymbol{q}} \sum_{\boldsymbol{k}} \left[\Delta_{\boldsymbol{q}}(\boldsymbol{k}) a^\dagger_{\boldsymbol{k}+\boldsymbol{q}/2\uparrow} a^\dagger_{-\boldsymbol{k}+\boldsymbol{q}/2\downarrow} + \Delta^*_{\boldsymbol{q}}(\boldsymbol{k}) a_{-\boldsymbol{k}+\boldsymbol{q}/2\downarrow} a_{\boldsymbol{k}+\boldsymbol{q}/2\uparrow} \right],$$

(5.4)

where we have defined the order parameter by

$$\Delta_{\boldsymbol{q}}(\boldsymbol{k}) = -\frac{1}{N} \sum_{\boldsymbol{k}'} V(\boldsymbol{k}, \boldsymbol{k}') \langle a_{-\boldsymbol{k}'+\boldsymbol{q}/2\downarrow} a_{\boldsymbol{k}'+\boldsymbol{q}/2\uparrow} \rangle,$$

(5.5)

with the bracket $\langle \cdots \rangle$ denoting the ensemble average. Using the Bogoliubov transformation

$$\begin{cases} a_{\boldsymbol{k}+\boldsymbol{q}/2\uparrow} = u_{\boldsymbol{k}} \alpha_{\boldsymbol{k}\uparrow} + v_{\boldsymbol{k}} \alpha^\dagger_{-\boldsymbol{k}\downarrow} \\ a^\dagger_{-\boldsymbol{k}+\boldsymbol{q}/2\downarrow} = u_{\boldsymbol{k}} \alpha^\dagger_{-\boldsymbol{k}\downarrow} - v_{\boldsymbol{k}} \alpha_{\boldsymbol{k}\uparrow}, \end{cases}$$

(5.6)

the gap equation is obtained as

$$\Delta_{\boldsymbol{q}}(\boldsymbol{k}') = \frac{1}{N} \sum_{\boldsymbol{k}} V(\boldsymbol{k}, \boldsymbol{k}') \frac{1 - f(E_{\boldsymbol{k}\uparrow}) - f(E_{\boldsymbol{k}\downarrow})}{2E_{\boldsymbol{k}}} \Delta_{\boldsymbol{q}}(\boldsymbol{k}),$$

(5.7)

where

$$\Delta_{\boldsymbol{q}}(\boldsymbol{k}) = \Delta_{\boldsymbol{q}} \gamma_\alpha(\boldsymbol{k}),$$

(5.8)

and $f(\epsilon)$ is the Fermi distribution function. Since the summation can be rewritten into the integral over the first Brillouin zone, we obtain

$$\Delta_{\boldsymbol{q}}(\boldsymbol{k}') = \int d\xi_{\boldsymbol{k}} \sum_{s=\pm} \int_{-\pi}^{\pi} \frac{dk_y}{2\pi} \rho(\xi_{\boldsymbol{k}}, k_y) \frac{1 - f(E_{\boldsymbol{k}\uparrow}) - f(E_{\boldsymbol{k}\downarrow})}{2E_{\boldsymbol{k}}} \Delta_{\boldsymbol{q}}(\boldsymbol{k}).$$

(5.9)

Here, we have defined the density of states $\rho(\xi_{\boldsymbol{k}}, k_y)$ by

$$\frac{1}{N} \sum_{\boldsymbol{k}} F(\boldsymbol{k}) = \int d\xi_{\boldsymbol{k}} \sum_{s=\pm} \int_{-\pi}^{\pi} \frac{dk_y}{2\pi} \rho(\xi_{\boldsymbol{k}}, k_y) F(\xi_{\boldsymbol{k}}, s, k_y),$$

(5.10)

for an arbitrary smooth function $F(\xi_{\boldsymbol{k}}, s, k_y) = F(\boldsymbol{k})$ with $s = \mathrm{sgn}(k_x)$, and $E_{\boldsymbol{k}\sigma} = \sigma\zeta + E_{\boldsymbol{k}}$ with $E_{\boldsymbol{k}} = \sqrt{\xi_{\boldsymbol{k}}^2 + \Delta_{\boldsymbol{q}}(\boldsymbol{k})^2}$ and

$$\zeta = h_{c2} \left(\frac{\boldsymbol{v}_{\mathrm{F}}(s, k_y) \cdot \boldsymbol{q}}{2h_{c2}} - 1 \right),$$

(5.11)

and $\boldsymbol{v}_\mathrm{F}(s, k_y)$ is the Fermi velocity. As mentioned above, the momentum dependence of $\boldsymbol{v}_\mathrm{F}(s, k_y)$ is taken into account. The integral with respect to $\xi_{\boldsymbol{k}}$ is taken over a region near the Fermi surface. Taking the limit $\Delta_{\boldsymbol{q}} \to 0$, we obtain the T_c equation as

$$
\begin{aligned}
\log \frac{T_\mathrm{c}^{(0)}}{T_\mathrm{c}} &= \int_0^\infty dt \sum_{s=\pm} \int_{-\pi}^{\pi} \frac{dk_y}{2\pi} \frac{\rho_\alpha(0, k_y)}{N_\alpha(0)} \\
&\quad \times \sinh^2 \frac{\beta\zeta}{2} \frac{\tanh t}{t \left[\cosh^2 t + \sinh^2(\beta\zeta/2)\right]},
\end{aligned}
\tag{5.12}
$$

where $\rho_\alpha(0, k_y) = \rho(0, k_y)\left[\gamma_\alpha(k_y)\right]^2$. The length of $\boldsymbol{q}$ is optimized so that T_c or H_{c2} is maximized. For numerical calculations, we rewrite Eq. (5.12) as

$$
\begin{aligned}
\log \frac{T_\mathrm{c}}{T_\mathrm{c}^{(0)}} &= -\sum_{s=\pm} \int_{-\pi}^{\pi} \frac{dk_y}{2\pi} \frac{\rho_\alpha(0, k_y)}{N_\alpha(0)} \sinh^2 \frac{\beta\zeta}{2} \int_0^\infty dy \log y \\
&\quad \times \left[\frac{2\sinh^2 y}{\left[\cosh^2 y + \sinh^2(\beta\zeta/2)\right]^2} - \frac{1}{\cosh^2 y \left[\cosh^2 y + \sinh^2(\beta\zeta/2)\right]} \right].
\end{aligned}
\tag{5.13}
$$

Here, we have defined an effective density of states at the Fermi energy for α-wave pairing $N_\alpha(0)$ is

$$
N_\alpha(0) = \sum_{s=\pm} \int_{-\pi}^{\pi} \frac{dk_y}{2\pi} \rho(0, k_y)[\gamma_\alpha(\boldsymbol{k})]^2,
\tag{5.14}
$$

with

$$
\rho(0, k_y) = \frac{1}{2\pi} \frac{1}{2t_a \sin\{k_{\mathrm{F}x}(k_y)\}},
\tag{5.15}
$$

where $k_{\mathrm{F}x}(k_y)$ is the value of k_x on the Fermi surface at k_y.

5.2. FFLO upper critical field at T = 0

In this subsection, the H_{c2} equation at $T = 0$ is derived. The normal and anomalous ground-state Green-functions are defined by

$$\begin{cases} G(t - t') = -i\langle T[a_{\boldsymbol{k}'\uparrow}(t)a_{\boldsymbol{k}\uparrow}^\dagger(t')]\rangle_0 \\ F^+(t - t') = i\langle T[a_{-\boldsymbol{k}'+\boldsymbol{q}\downarrow}^\dagger(t)a_{\boldsymbol{k}\uparrow}^\dagger(t')]\rangle_0, \end{cases} \tag{5.16}$$

where $\langle \hat{A}\rangle_0$ denotes the quantum mechanical expectation value of the operator $\hat{A}$ in the ground state. Here, $T[\cdots]$ and t are the time-ordering symbol and time, respectively. The equations of motion of the Green functions are

$$\begin{cases} i\dfrac{\partial}{\partial t}G(t - t') = \delta(t - t')\delta_{\boldsymbol{k},\boldsymbol{k}'} - i\langle T[[a_{\boldsymbol{k}'\uparrow}(t), H]a_{\boldsymbol{k}\uparrow}^\dagger(t')]\rangle_0 \\ i\dfrac{\partial}{\partial t}F^+(t - t') = i\langle T[[a_{-\boldsymbol{k}'+\boldsymbol{q}\downarrow}^\dagger(t), H]a_{\boldsymbol{k}\uparrow}^\dagger(t')]\rangle_0. \end{cases} \tag{5.17}$$

Using Eq. (5.4), the gap equations are derived. By the Fourier transformation Eq. (5.17) is written as

$$\begin{cases} (\omega + i\delta\omega + \xi_{-\boldsymbol{k}+\boldsymbol{q}} + h)F_\omega^+(\boldsymbol{k}) + \Delta_{\boldsymbol{q}}^*(\boldsymbol{k})G_\omega(\boldsymbol{k}) = 0 \\ (\omega + i\delta\omega - \xi_{\boldsymbol{k}} + h)G_\omega(\boldsymbol{k}) + \Delta_{\boldsymbol{q}}(\boldsymbol{k})F_\omega^+(\boldsymbol{k}) = 1, \end{cases} \tag{5.18}$$

where

$$\Delta_{\boldsymbol{q}}(\boldsymbol{k}) = -\frac{1}{N}\sum_{\boldsymbol{k}'}V(\boldsymbol{k}, \boldsymbol{k}')\langle a_{-\boldsymbol{k}'+\boldsymbol{q}\downarrow}a_{\boldsymbol{k}'\uparrow}\rangle_0. \tag{5.19}$$

Therefore, the ground state gap equation is obtained as

$$\begin{aligned} \Delta_{\boldsymbol{q}}^*(\boldsymbol{k}') &= \frac{1}{N}\sum_{\boldsymbol{k}}\int_{-\infty}^{\infty}\frac{d\omega}{2\pi i}V(\boldsymbol{k}, \boldsymbol{k}') \\ &\times \frac{\Delta_{\boldsymbol{q}}^*(\boldsymbol{k})}{(\omega + i\delta\omega - \xi_{\boldsymbol{k}} + h)(-\omega - i\delta\omega - \xi_{-\boldsymbol{k}+\boldsymbol{q}} - h) + |\Delta_{\boldsymbol{q}}(\boldsymbol{k})|^2}. \end{aligned} \tag{5.20}$$

Taking the limit $\Delta_{\boldsymbol{q}} \to 0$, we obtain the H_{c2} equation:

$$1 - V_\alpha\int_{-\infty}^{\infty}\frac{d\omega}{2\pi i}\int\frac{d^2\boldsymbol{k}}{(2\pi)^2}[\gamma_\alpha(\boldsymbol{k})]^2\frac{1}{(\omega + i\delta\omega - \xi_{\boldsymbol{k}} + h)(-\omega - i\delta\omega - \xi_{-\boldsymbol{k}+\boldsymbol{q}} - h)} = 0. \tag{5.21}$$

The upper critical field at $T = 0$ is obtained by solving

$$h_{c2} = \frac{\Delta_{\alpha 0}}{2}\exp\left[-\sum_{s=\pm}\int_{-\pi}^{\pi}\frac{dk_y}{2\pi}\frac{\rho_\alpha(0, k_y)}{N_\alpha(0)}\log\left|1 - \frac{\boldsymbol{v}_F(s, k_y)\cdot\boldsymbol{q}}{2h_{c2}}\right|\right], \tag{5.22}$$

where the FFLO vector $\boldsymbol{q}$ is optimized so that the h_{c2} is maximized [9, 10]. Here, $h_{c2} = \mu_e H_{c2}$, $\Delta_{\alpha 0} = 2\omega_c\exp[-1/|V_\alpha|N_\alpha(0)]$, and ω_c is the cutoff frequency.

5.3. Pauli paramagnetic limit at finite temperatures

In the following two subsections, we formulate the H_P equation. The free energies F_0 for the BCS state ($\boldsymbol{q} = 0$) in magnetic field is obtained from the partition function for the mean field Hamiltonian Eq. (5.4),

$$
\begin{aligned}
F_0 = &- 2k_B T \sum_{\boldsymbol{k}} \ln(1 + e^{-\beta E_{\boldsymbol{k}}}) \\
&+ \sum_{\boldsymbol{k}} \left[\xi_{\boldsymbol{k}} - E_{\boldsymbol{k}} + \left[\Delta_0(\boldsymbol{k})\right]^2 \frac{1 - f(E_{\boldsymbol{k}\uparrow}) - f(E_{\boldsymbol{k}\downarrow})}{2E_{\boldsymbol{k}}} \right],
\end{aligned}
\tag{5.23}
$$

where $\Delta_0(\boldsymbol{k}) = \Delta_0(T)\gamma_\alpha(\boldsymbol{k})$. When $\Delta_0(T) = 0$, this free energy is reduced to the normal-state free-energy F_n:

$$
F_n = -2k_B T \sum_{\boldsymbol{k}} \ln(1 + e^{-\beta \xi_{\boldsymbol{k}}}) + \sum_{\boldsymbol{k}} \left[\xi_{\boldsymbol{k}} - |\xi_{\boldsymbol{k}}| \right].
\tag{5.24}
$$

The difference of the free energies $\Delta F \equiv F_0 - F_n$ is written as

$$
\begin{aligned}
\Delta F = &\, T \sum_{\boldsymbol{k}\sigma} \ln \frac{1 + e^{-\beta(\sigma h_P + |\xi_{\boldsymbol{k}}|)}}{1 + e^{-\beta(\sigma h_P + \sqrt{\xi_{\boldsymbol{k}}^2 + \Delta_0(\boldsymbol{k})^2})}} \\
&- \frac{1}{2} N N_\alpha(0) \left[\Delta_0(T)\right]^2 \left(1 + 2\ln\left|\frac{\Delta_\alpha^{(0)}}{\Delta_0(T)}\right|\right).
\end{aligned}
\tag{5.25}
$$

Then, the H_P and $\Delta_0(T)$ equation is obtained from the condition $\Delta F = 0$ as

$$
\begin{aligned}
\int_{-\pi}^{\pi} \frac{dk_y}{2\pi} \rho(0, k_y) \left(\frac{h_P}{\Delta_{\alpha 0}}\right)^2 = &\, \frac{N_\alpha(0)}{2} \left(\frac{\Delta_0(T)}{\Delta_{\alpha 0}}\right)^2 \left(1 + 2\ln\left|\frac{\Delta_\alpha^{(0)}}{\Delta_0(T)}\right|\right) \\
&- \frac{2T}{\Delta_{\alpha 0}} \frac{\Delta_0(T)}{\Delta_{\alpha 0}} \int_{-\pi}^{\pi} \frac{dk_y}{2\pi} \rho(0, k_y) \gamma_\alpha(\boldsymbol{k}) \\
&\times \sum_\sigma \int_0^\infty dp \, \cosh p \, \ln\left(\frac{1 + e^{-\beta|\sigma h_P + \Delta_0(\boldsymbol{k})\sinh p|}}{1 + e^{-\beta|\sigma h_P + \Delta_0(\boldsymbol{k})\cosh p|}}\right),
\end{aligned}
\tag{5.26}
$$

where $\Delta_\alpha^{(0)}$ is the order parameter at $T = 0$ determined by the gap equation (5.7).

On the other hand, a gap equation for $\boldsymbol{q} = 0$ written as

$$
\ln\left(\frac{\Delta_\alpha^{(0)}}{\Delta_0(T)}\right) = \int_{-\pi}^{\pi} \frac{dk_y}{2\pi} \frac{\rho_\alpha(0, k_y)}{N_\alpha(0)} \sum_\sigma \int_0^\infty dp \, \frac{1}{e^{\beta(\sigma h_P + \Delta_0(\boldsymbol{k})\cosh p)} + 1}.
\tag{5.27}
$$

Solving Eqs. (5.26) and (5.27) numerically, $\Delta_0(T)$ and H_P are obtained.

5.4.   Pauli paramagnetic limit at $\mathbf{T = 0}$

The superconducting condensation energy ΔE is determined by Eq. (5.25) at $T = 0$ and $H = 0$. Therefore, ΔE is written as $[N N_\alpha(0)|\Delta_\alpha^{(0)}|^2]/2$. The Pauli paramagnetic limit H_{P} at $T = 0$ is determined by the condition that the spin polarization energy is equal to the superconducting condensation energy as

$$\chi \frac{H_{\mathrm{P}}{}^2}{2} = \frac{N_\alpha(0)|\Delta_\alpha^{(0)}|^2}{2}, \tag{5.28}$$

where χ is the spin susceptibility, and

$$\Delta_\alpha^{(0)} = \frac{1}{\bar{\gamma}_\alpha}\Delta_{\alpha 0} \tag{5.29}$$

with

$$\frac{1}{\bar{\gamma}_\alpha} = \exp\left[\frac{\sqrt{\left\langle\left[\gamma_\alpha(\boldsymbol{k})\right]^2 \log\left[1/|\gamma_\alpha(\boldsymbol{k})|\right]\right\rangle_{\mathrm{F}}}}{\sqrt{\left\langle\left[\gamma_\alpha(\boldsymbol{k})\right]^2\right\rangle_{\mathrm{F}}}}\right]. \tag{5.30}$$

Here, we have defined the average over Fermi surface:

$$\langle \cdots \rangle_{\mathrm{F}} = \int_{-\pi}^{\pi}\frac{dk_y}{2\pi}\frac{\rho(0, k_y)}{N(0)}(\cdots). \tag{5.31}$$

$N(0)$ denotes the density of states. The Pauli paramagnetic limits for s- and d-wave pairing are derived as

$$\begin{cases} \dfrac{h_{\mathrm{P}}}{\Delta_{\mathrm{d}0}} = \dfrac{\sqrt{\left\langle\left[\gamma_{\mathrm{d}}(\boldsymbol{k})\right]^2\right\rangle}}{\bar{\gamma}_{\mathrm{d}}}\dfrac{1}{\sqrt{2}} \\[3mm] \dfrac{h_{\mathrm{P}}}{\Delta_{\mathrm{s}0}} = \dfrac{1}{\sqrt{2}}, \end{cases} \tag{5.32}$$

where $h_{\mathrm{P}} = \mu_{\mathrm{e}}H_{\mathrm{P}}$

6.   NUMERICAL RESULTS

6.1.   FFLO upper critical fields at finite temperatures

In this subsection, the numerical results for the temperature dependences of the upper critical fields are shown assuming s-wave and d-wave pairings. First, we consider the modulation vector $\boldsymbol{q} \parallel \boldsymbol{a}$, which direction of $\boldsymbol{q}$ seems favorable for Fermi-surface nesting, since the Fermi surfaces touch by the shortest $\boldsymbol{q}$, and thus the spatial variation in $\Delta(\boldsymbol{r})$ is minimum. In fact, this is confirmed below by numerical calculations.

Figure 7 (a) shows the temperature dependence of the upper critical fields for d-wave pairing. For $t_b/t_a \lesssim 0.1$, we find a new kind of dimensional crossover as follows. Just below the tricritical temperature T^*, the upper critical field $H_{c2}(T)$ increases steeply along the curve of the 1D system. However, with the temperature decreased, the rate of increase in $H_{c2}(T)$ diminishes, and a shoulder appears. The behavior of $H_{c2}(T)$ at lower temperatures is reduced to that in the 2D systems, i.e., an upturn and a finite value at $T = 0$. The shoulder becomes less pronounced for $t_b/t_a \sim 0.15$ and completely disappears for $t_b/t_a \sim 0.25$. Independently of the value of $t_b/t_a \neq 0$, the low-temperature behavior is essentially that of a Q2D system and thus classified as type (b). As t_b/t_a increases, the FFLO upper critical field decreases, and for $t_b/t_a \gtrsim 0.25$, the upper critical field is lower than that in 2D isotropic systems.

Figure 7 (b) shows the temperature dependence of the optimized $q \equiv |\boldsymbol{q}|$ at the magnetic field $H = H_{c2}(T)$. Below $T \approx 0.56 \times T_c$, the FFLO state $\boldsymbol{q} \neq 0$ occurs. The behavior of q is not monotonic, which reflects the behavior of $H_{c2}(T)$. As shown in the left figure, all curves of $\bar{q} \equiv v_{F0}q/2h$ converge to unity at $T = 0$, where $v_{F0} \equiv |v_{Fx}(s, k_y = 0)|$. From this convergence, the Fermi surfaces touch on a line at $k_y = 0$ by the transformation $\boldsymbol{k} \to -\boldsymbol{k} + \boldsymbol{q}$ of the spin-down Fermi surface.
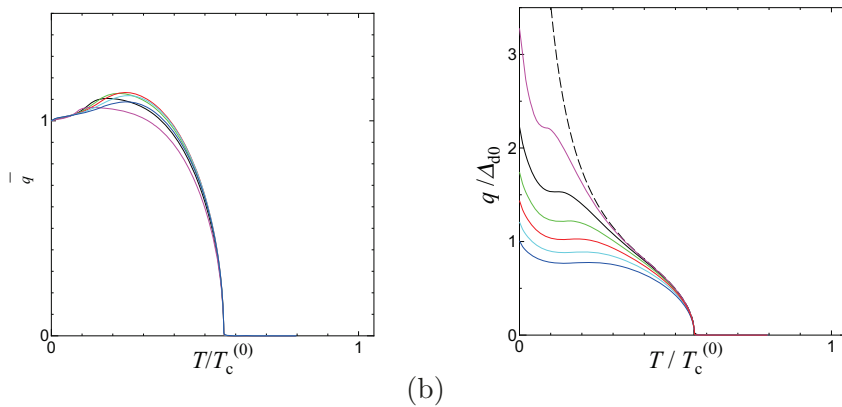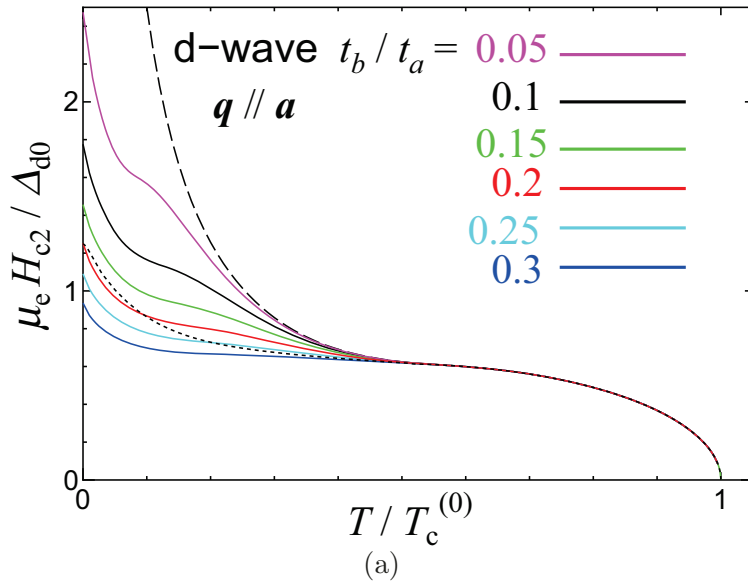
FIG. 7: Temperature dependence of the upper critical field and q for d-wave pairing when $t_b/t_a = 0.1$ (from Ref. [40]). The solid curves show the results for the range of φ from 0 to $\pi/2$. The dashed curve is for a 1D system. The dotted curve is for a 2D isotropic system with $d_{x^2-y^2}$-wave pairing when $\boldsymbol{q} \parallel \hat{\boldsymbol{x}}$.

Figure 8 (a) shows the temperature dependence of the upper critical field for s-wave pairing. Similar to that for d-wave pairing, a dimensional crossover from one dimension to two dimensions is found. However, the upturn at low temperatures is weaker than that for d-wave pairing. This difference originates from the difference in the Fermi-surface nesting. For $\boldsymbol{q} \parallel \boldsymbol{a}$, the Fermi surfaces touch on a line at $k_y = 0$,

where the amplitude of the gap function is maximum for d-wave pairing.

Figure 8 (b) shows the temperature dependence of q. As shown in the left figure, all curves of $\bar{q}$ converge to unity at $T = 0$, which implies that the Fermi surfaces touch on a line at $k_y = 0$. This behavior is the same as that for d-wave pairing.

(a)

(b)
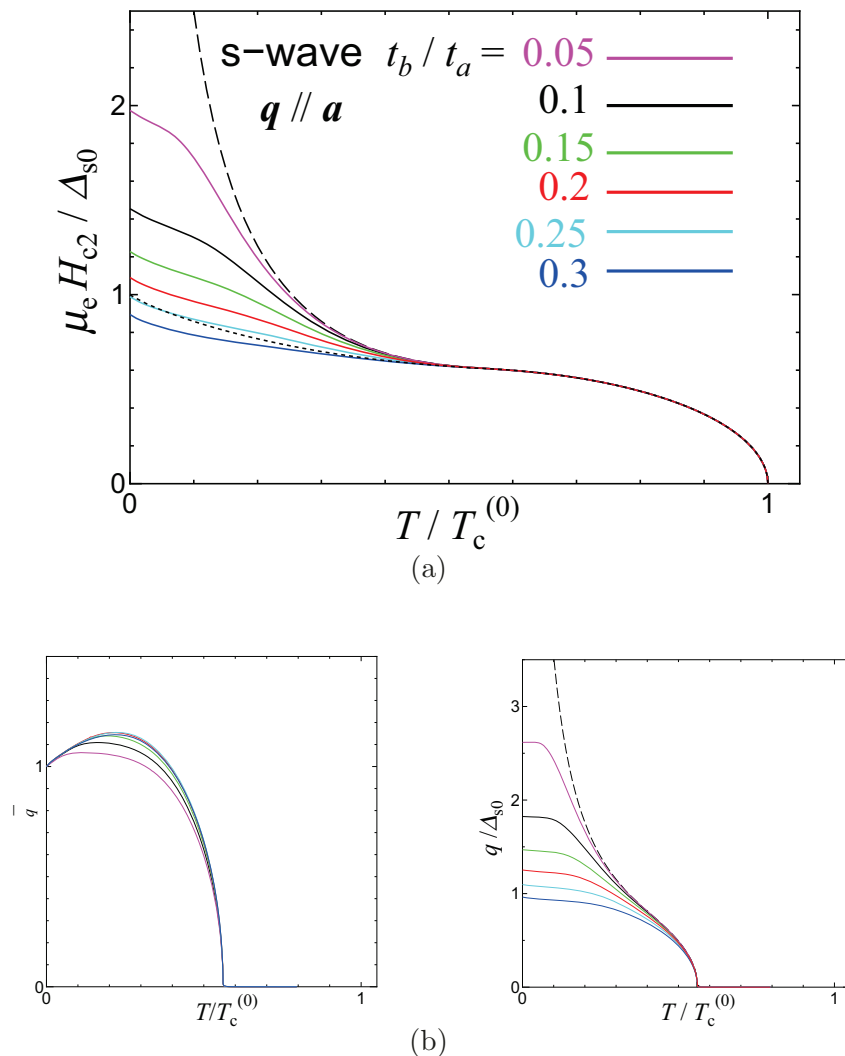
FIG. 8: Temperature dependence of the upper critical field and q for s-wave pairing when $q \parallel a$ (from Ref. [40]). The solid curves are for the range of t_b/t_a from 0.05 to 0.3. The dashed curve plots a 1D system at $t_b = 0$. The dotted curve is for a 2D isotropic system with s-wave pairing.

Next, we consider the dependence of $H_{c2}(T)$ on the direction of the FFLO mod-

ulation vector $\boldsymbol{q}$. Figure 9 shows the results for d-wave pairing when $t_b/t_a = 0.1$. The upturn in the low-temperature region disappears for $\varphi \gtrsim \pi/4$, but the large shoulder remains. This behavior can be interpreted in terms of the nesting concept. For a large angle $\varphi \gtrsim \pi/4$, the nesting condition of crossing along lines becomes more effective than that of touching on a line near the node of the d-wave gap function. Therefore, the low-temperature behavior is classified as type (c), but the magnitude is much larger than that in three-dimensional (3D) isotropic systems, because the crossing angle between the Fermi surfaces is extremely small owing to the Q1D Fermi-surface structure. The large shoulder vanishes between $\varphi = 7\pi/20$ and $9\pi/20$. The dimensional crossover between one and two dimensions appears only for $\varphi \lesssim 3\pi/20$.

The FFLO critical field is low when $\varphi = \pi/2$. Considering the factors that suppress the FFLO state, particularly the orbital pair-breaking effect, this result suggests that FFLO modulation does not occur in directions $\varphi \approx \pi/2$ in the Q1D materials. Therefore, in the compound $(TMTSF)_2ClO_4$, if the high-field phase for $\boldsymbol{H} \parallel \boldsymbol{b}'$ is an FFLO state, the modulation along $\boldsymbol{q}$ and the vortices along $\boldsymbol{H}$ cannot coexist in the form $\boldsymbol{q} \parallel \boldsymbol{H}$. In such a case, the Abrikosov functions with higher Landau-level indexes would contribute to the state, and the spatial modulation perpendicular to the magnetic field would be partly due to a paramagnetic effect [41, 52].
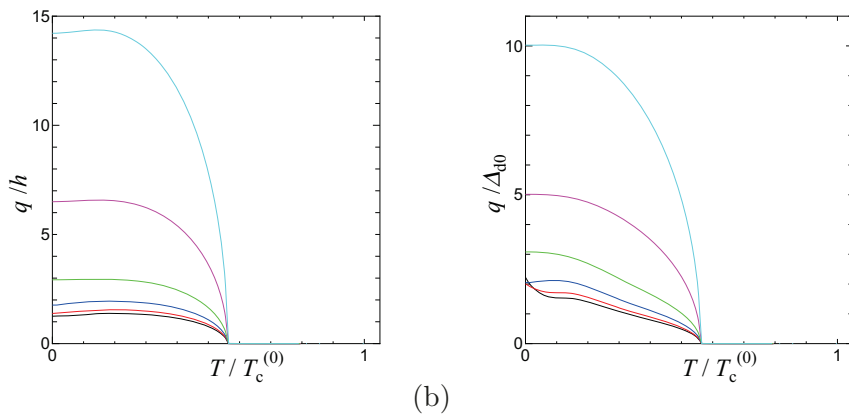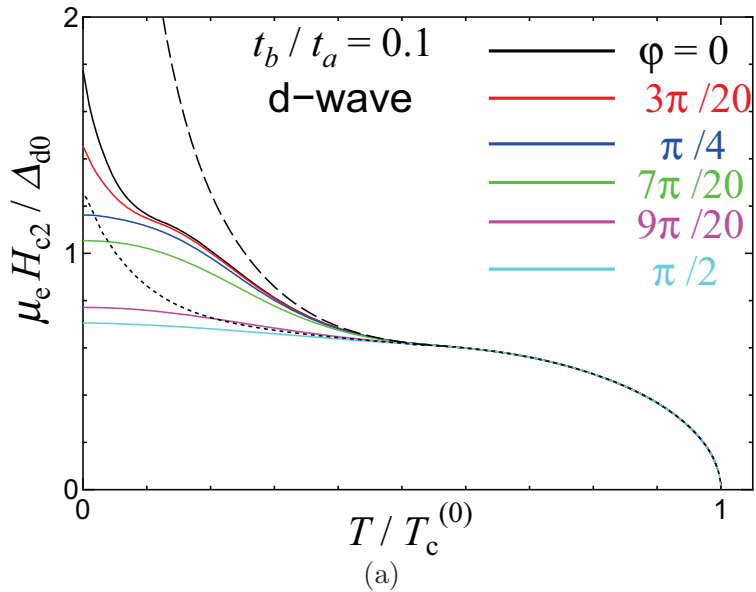
FIG. 9: Temperature dependence of the upper critical field and q for d-wave pairing when $t_b/t_a = 0.1$ (from Ref. [40]). The solid curves show the results for the range of φ from 0 to $\pi/2$. The dashed curve is for a 1D system. The dotted curve is for a 2D isotropic system with $d_{x^2-y^2}$-wave pairing when $\boldsymbol{q} \parallel \hat{\boldsymbol{x}}$.

Figure 10 shows the results for s-wave pairing when $t_b/t_a = 0.1$. Similar to the result for d-wave pairing, a steep increase occurs just below T^* for $\varphi \lesssim 7\pi/20$, but the upturn at low temperatures occurs for all φ's. It is found that q/h is equal to t_a/t_b at $T = 0$.
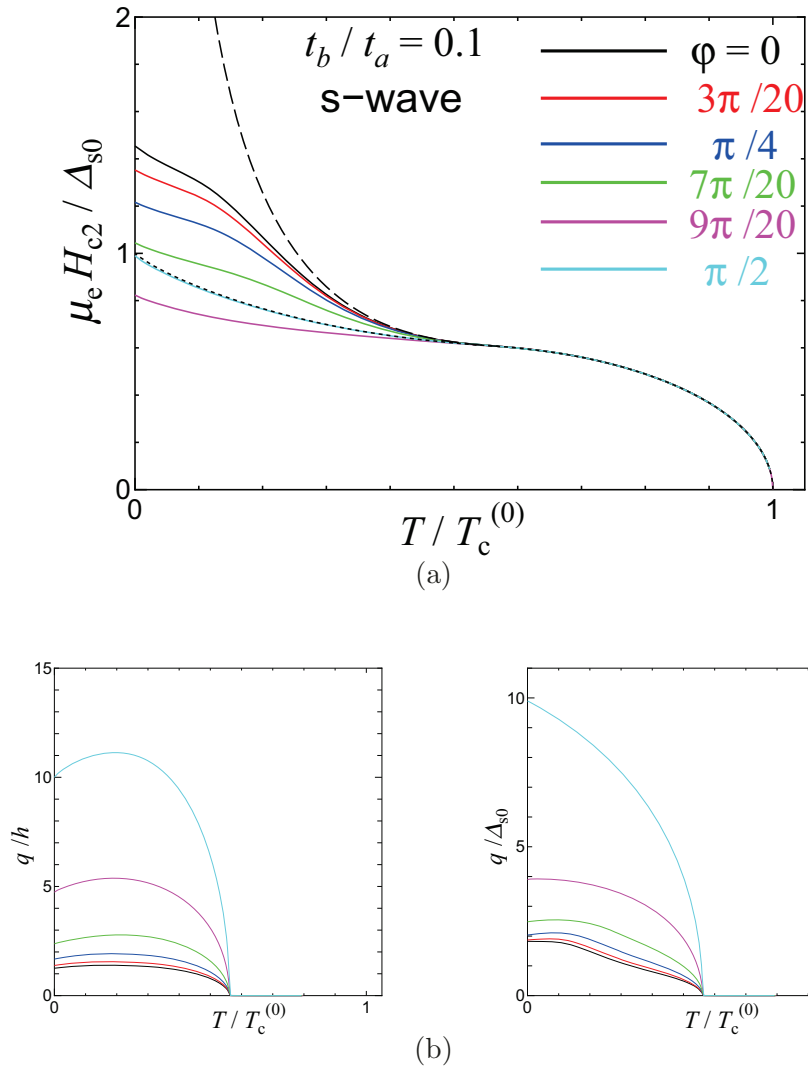
FIG. 10: Temperature dependence of the upper critical field and q for s-wave pairing when $t_b/t_a = 0.1$ (from Ref. [40]). The solid curves show the results for the range of φ from 0 to $\pi/2$. The dashed curve presents the result for a 1D system. The dotted curve is for a 2D isotropic system with s-wave pairing.

Figure 11 presents the results for d-wave pairing when $t_b/t_a = 0.2$. $H_{c2}(T)$ is maximum for $\varphi = 0$ in the whole temperature range. The nesting condition is "crossing along the lines" as that in the 3D systems for $\varphi \gtrsim \pi/4$ and the $dH_{c2}(0)/dT = 0$. When $\varphi \approx \pi/2$, the $H_{c2}(T)$ is not strongly affected by the latio t_b/t_a in contrast to $\varphi \approx 0$. The result is qualitatively the same as that for $t_b/t_a = 0.1$, except that the

value of q is smaller.
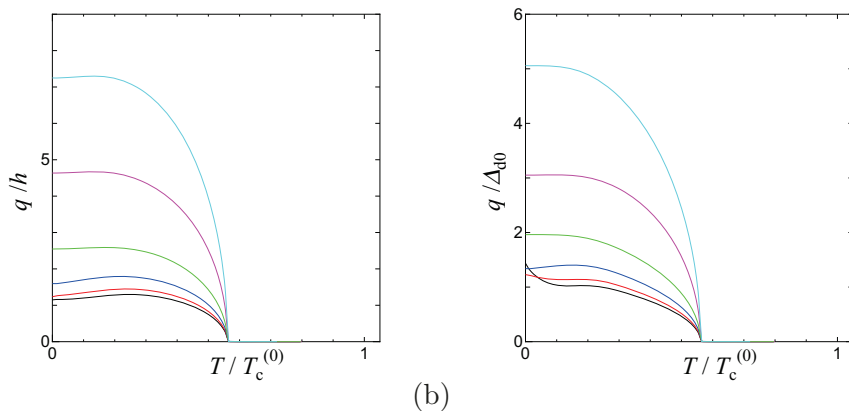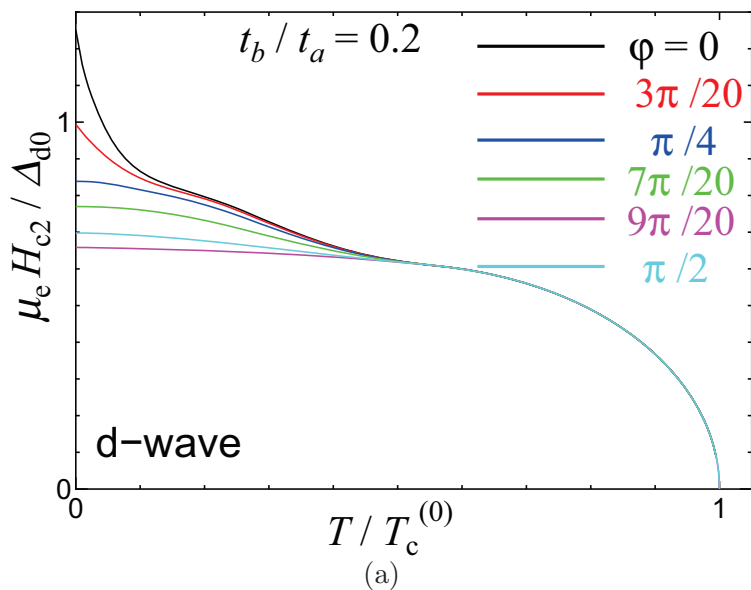
FIG. 11: Temperature dependence of the upper critical field and q for d-wave pairing when $t_b/t_a = 0.2$. The solid curves show the results for the range of φ from 0 to $\pi/2$.

Figure 12 graphs the results for s-wave pairing when $t_b/t_a = 0.2$. For $\varphi \lesssim 9\pi/20$, as angle φ increases, the upper critical fields $H_{c2}(T)$ decrease. In contrast, $H_{c2}(T)$ rapidly increases for $9\pi/20 < \varphi < \pi/2$. When $\varphi = \pi/2$, $H_{c2}(T)$ exceeds that for $\varphi = \pi/4$ at low temperatures.
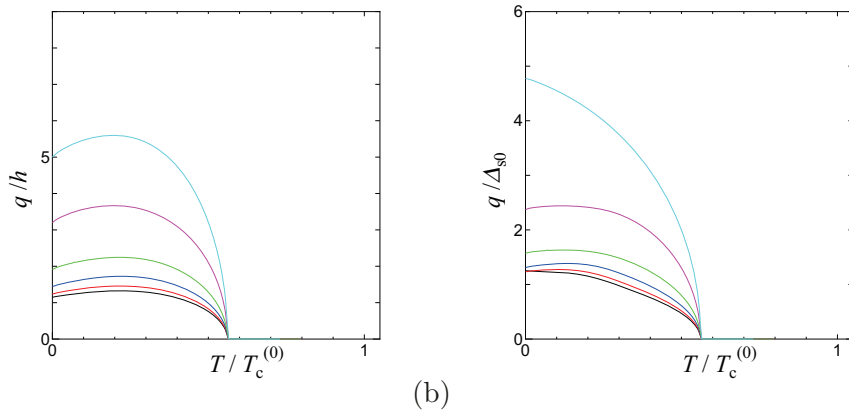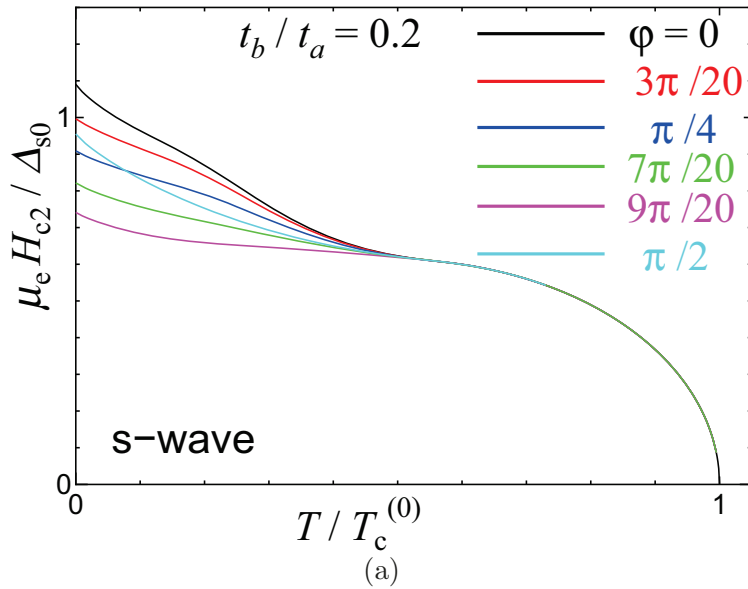
FIG. 12: Temperature dependence of the upper critical field and q for s-wave pairing when $t_b/t_a = 0.2$. The solid curves show the results for the range of φ from 0 to $\pi/2$.

Figure 13 shows the results for d-wave pairing when $t_b/t_a = 0.3$. For $\varphi \lesssim 3\pi/20$, a small upturn remains. When $\varphi = \pi/4$, the upper critical field is slightly higher than the Pauli paramagnetic limit. For $\varphi \approx 9\pi/20$, the upper critical field is slightly lower than the Pauli paramagnetic limit at $T = 0$.
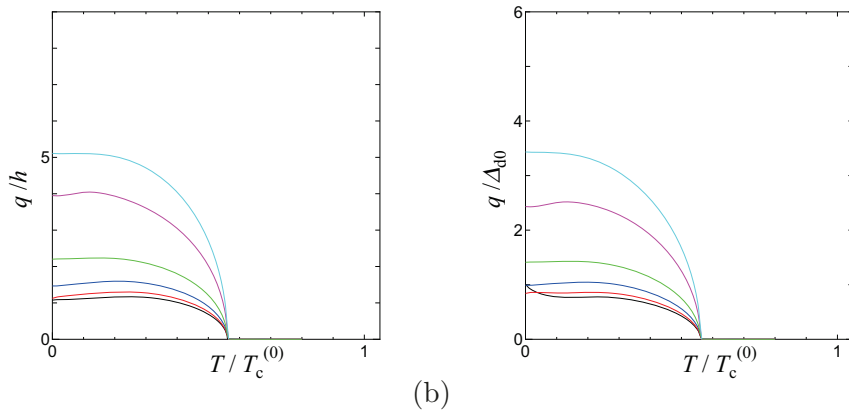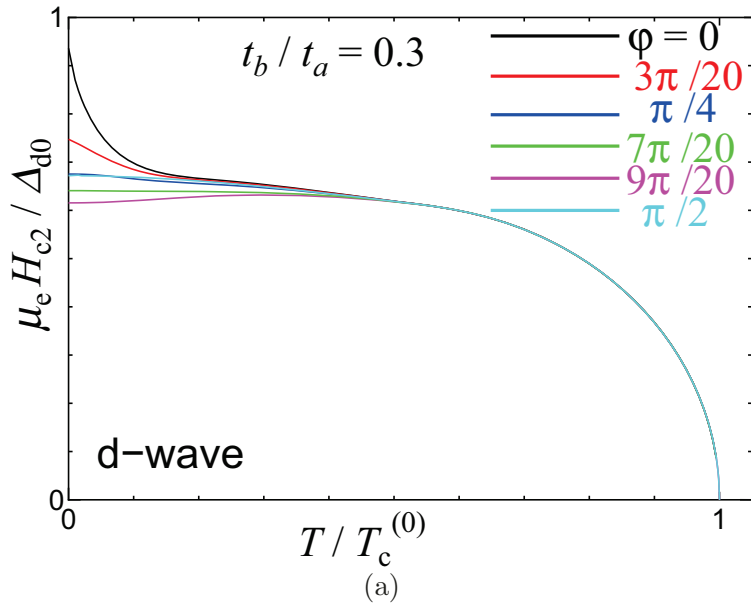
FIG. 13: Temperature dependence of the upper critical field and q for d-wave pairing when $t_b/t_a = 0.3$. The solid curves show the results for the range of φ from 0 to $\pi/2$.

Figure 14 presents the results for s-wave pairing when $t_b/t_a = 0.3$. The value of H_{c2} for $\varphi = \pi/2$ is near that for $\varphi = 0$. As a mentioned above, the upper critical field is maximum when $\boldsymbol{q} \parallel \boldsymbol{a}$, independently of $t_b/t_a \neq 0$.
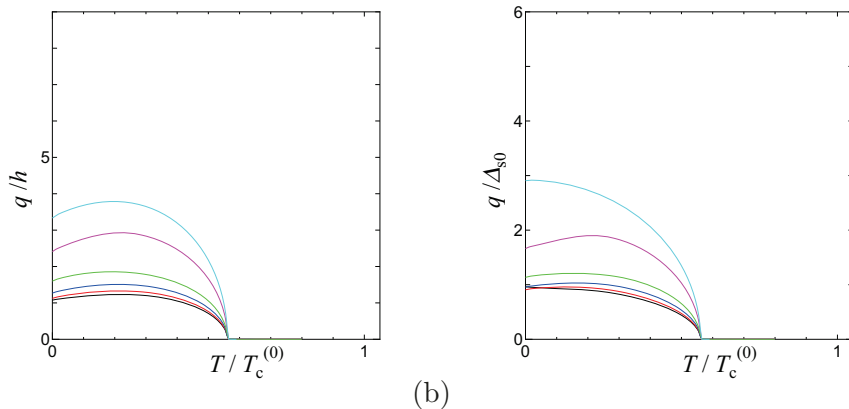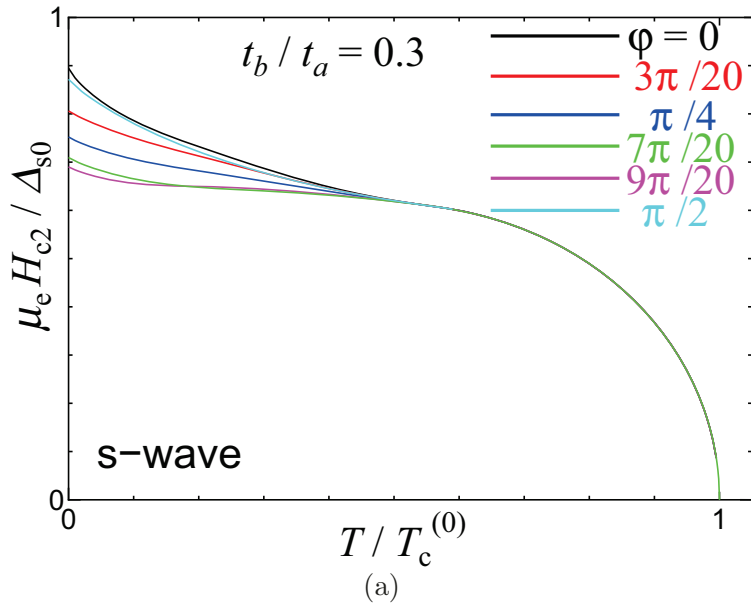
FIG. 14: Temperature dependence of the upper critical field and q for s-wave pairing when $t_b/t_a = 0.3$. The solid curves show the results for the range of φ from 0 to $\pi/2$.

In Fig. 15, we compare the theoretical curve and experimental data for $\boldsymbol{H} \parallel \boldsymbol{a}$. The present theory neglects the strong coupling effect, impurity (disorder) pair breaking, and thermal fluctuations in the Q1D system. In particular, in the presence of these effects, the ratio $\Delta_0/T_c^{(0)}$ would become larger than the weak coupling value of 1.76, where Δ_0 is the superconducting gap at $T = 0$ and $H = 0$. The simplest way to take these effects into account is to change the ratio of the scaling of the $T/T_c^{(0)}$ and H/Δ_0 axes. Therefore, in order to compare the present result and

the experimental data, we introduce the ratio $r = (\Delta_0^{\text{true}}/T_c^{\text{true}})/(\Delta_{d0}/T_c^{(0)})$, where Δ_0^{true} and T_c^{true} are the true values of Δ_0 and $T_c^{(0)}$, respectively.

In the experimental data [25, 26], H_{c2} saturates near $T = 0.7$ K and $H = 3$ T, reflecting the paramagnetic limit [53], but the increase in $H_{c2}(T)$ recovers below $T \approx 0.3$ K. Hence, a tricritical point (T^*, H^*) should exist above $T = 0.3$ K if the recovery is owing to the emergence of a different superconducting phase such as the FFLO state. As shown in Fig. 15, the experimental data for T_c can be fitted by a fourth-order polynomial in H over a region near and above H^*. As a result, a small shoulder appears below $T = 0.2$ K, corresponds to the present theory. The point at which $\mathrm{d}^2 T(H)/\mathrm{d}H^2$ changes its sign is the tricritical point. The values obtained from the least-squares fit are $T^* \approx 0.42$ K and $H^* \approx 3.7$ T. The difference between this T^* and the theoretical $T^* = 0.56 \times T_c \approx 0.81$ K is owing to the orbital pair-breaking effect. In the present theory, $H_{c2}(T)$ exhibits a second steep increase below the shoulder near $T = 0$ for d-wave pairing, while it does not for s-wave pairing. The complex behavior of $H_{c2}(T)$ for d-wave pairing is owing to the nesting effect in a Q1D system, reflecting the structure of the d-wave gap function with line nodes near $k_y = \pm\pi/2$. Hence, unless the orbital effect is too strong, the second steep increase that indicates a d-wave FFLO state might be observed near $T = 0$ for $\boldsymbol{H} \parallel \boldsymbol{a}$.
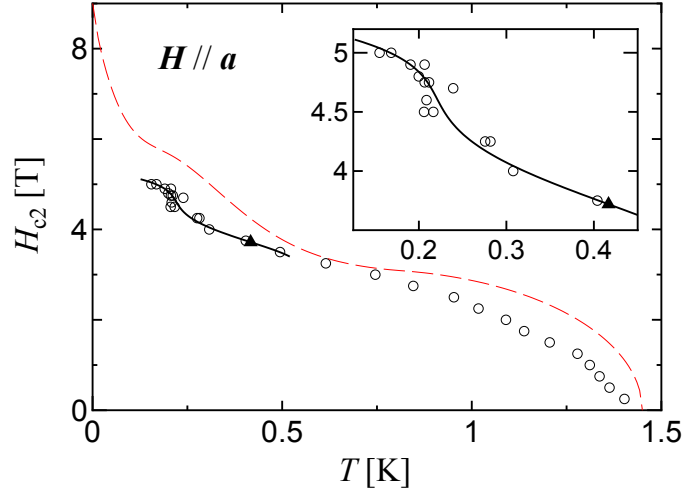
FIG. 15: Comparison of the theoretical results with the experimental data [25, 26] for $H \parallel a$. The solid curve is from a least-squares fit of the transition temperatures to a fourth-order polynomial in H below $T = 0.5$ K. The red dashed curve is the theoretical result for d-wave pairing with $t_b/t_a = 0.1$, $\varphi = 0$, and $g/r = 1.5$, where g and r are the g-factor and a factor taking into account the correction of the ratio $\Delta_0/T_c^{(0)}$, respectively. The closed triangle indicates the tricritical point determined by the least-squares fit. (From Ref. [40].)

6.2. FFLO upper critical field at T = 0

In this subsection, we present the results of the upper critical fields and the nesting conditions at $T = 0$. Figure 16 plots $H_{c2}(0)$ as a function of the angle φ for d-wave pairing. It is found that the direction $\boldsymbol{q} \parallel \boldsymbol{a}$ i.e. $\varphi = 0$ is the most favorable, because of the nesting effect, for both d-wave and s-wave pairings. This remains unchanged at finite temperatures. For $\varphi \gtrsim \pi/4$, the nesting condition of "crossing along lines" becomes more effective than that of "touching on a line" near the node. Thus, a non-monotonic behavior in $H_{c2}(0)$ is observed for $\varphi \approx \pi/4$.

Figure 17 presents φ dependence of the upper critical fields for s-wave pairing. $H_{c2}(0)$ decreases simply up to $\varphi \approx 9\pi/20$. More than $\varphi \approx 9\pi/20$, $H_{c2}(0)$ shows a small increase. This behavior can be interpreted in terms of the nesting concept. For $\varphi \lesssim 9\pi/20$, nesting condition of touching on the right Fermi surface is favorable. For $\varphi \gtrsim 9\pi/20$, nesting condition of touching on the left surface becomes more effective than that of touching on the right surface (see fig. 20).
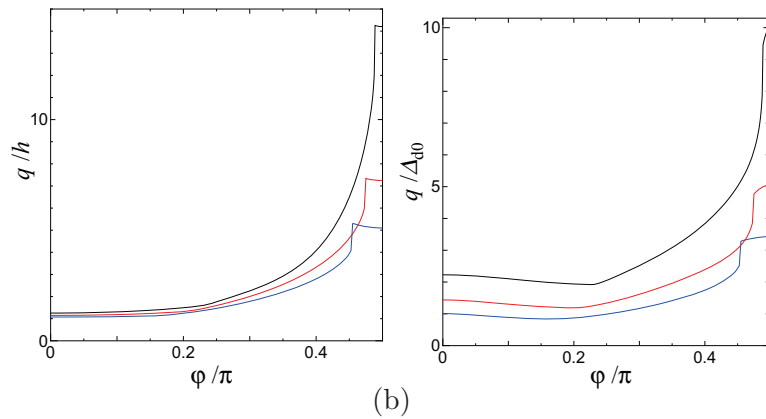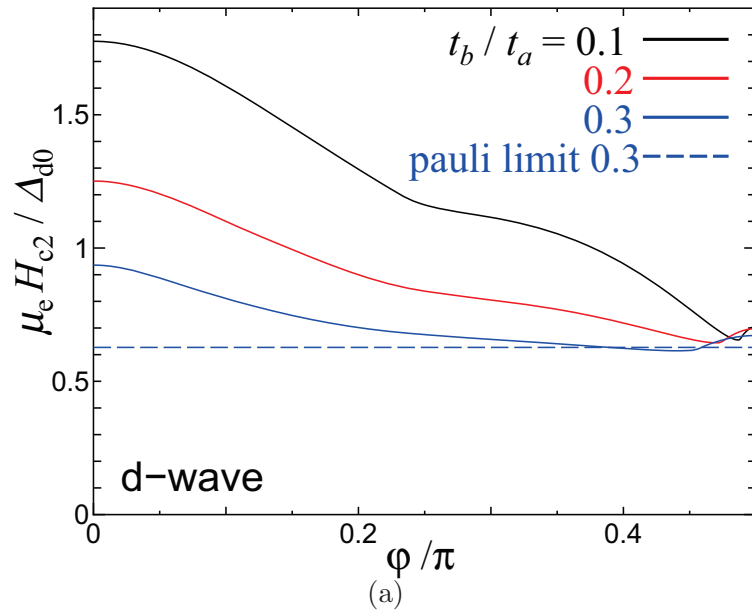
FIG. 16: Angle φ dependence of the upper critical fields and q at $T = 0$ (from Ref. [40]). The curves show the results for d-wave pairing. The dashed curve shows the Pauli paramagnetic limit for d-wave pairing with $t_b/t_a = 0.3$.
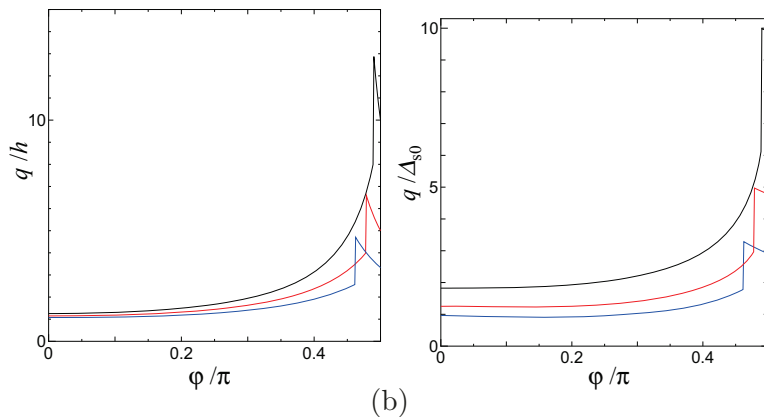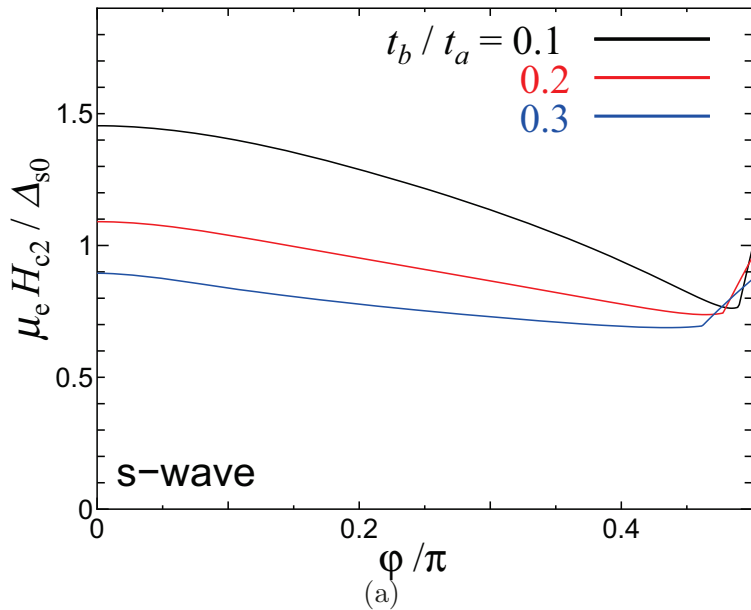
FIG. 17: Angle φ dependence of the upper critical fields and q at $T = 0$ for s-wave pairing (from Ref. [40]).

Figure 18 shows the Fermi-surface nesting conditions for s- and d-wave pairings and for $t_b/t_a = 0.1$ and 0.2. The nesting conditions of both s- and d-wave pairing are "touch on a line or lines" as in the Q2D systems at $k_y = 0$ and they are not the perfect nesting, independently of the ratio t_b/t_a. It has been proved that the difference between the Fermi surface of spin-up elections shifted by $\boldsymbol{q}$ and that of spin-down electrons is proportional to $t_b T_c^{(0)}/t_a$ in section 3.
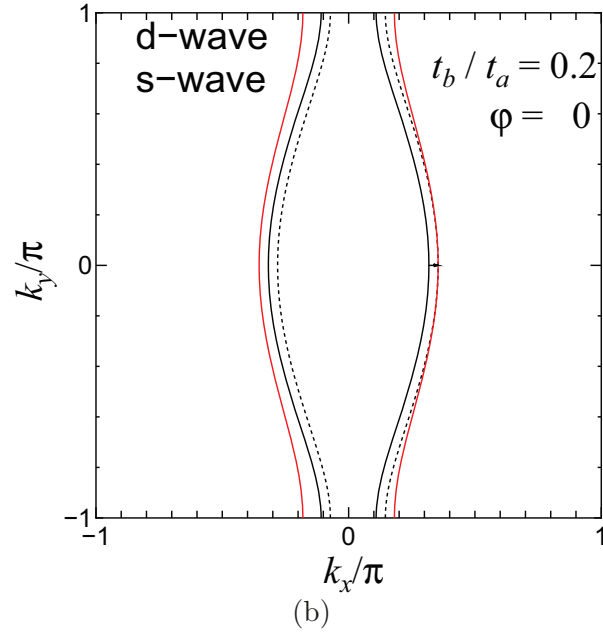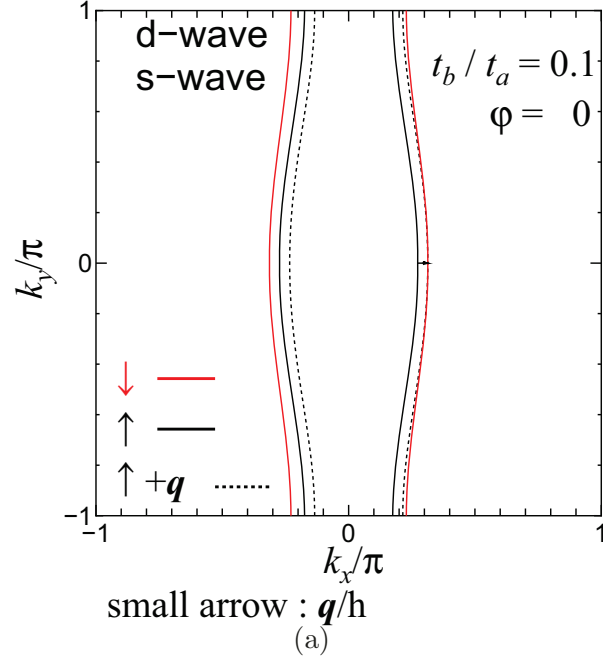
FIG. 18: Nesting conditions for s- and d-wave pairing, when $q \parallel a$. Black and red solid line are the Fermi surfaces of spin-up electrons and spin-down electrons, respectively. Dotted curves show spin-up electrons shifted by q. The small arrow shows q/h, and connects the points on the Fermi surfaces which touch by the transition $k \to k+q$. Figure (a) and (b) plot the case of $t_b/t_a = 0.1$ and 0.2, respectively.

Figure 19 presents the nesting condition for d-wave pairing and for several values of the angle φ at $T = 0$. For $\varphi \gtrsim \pi/4$, it is obtained that $dH_{c2}(0)/dT = 0$, and the nesting condition is "crossing along lines" as in the 3D systems. This change relates to the non-monotonic behavior observed in the angle φ dependence of $H_{c2}(0)$ in $(TMTSF)_2ClO_4$.
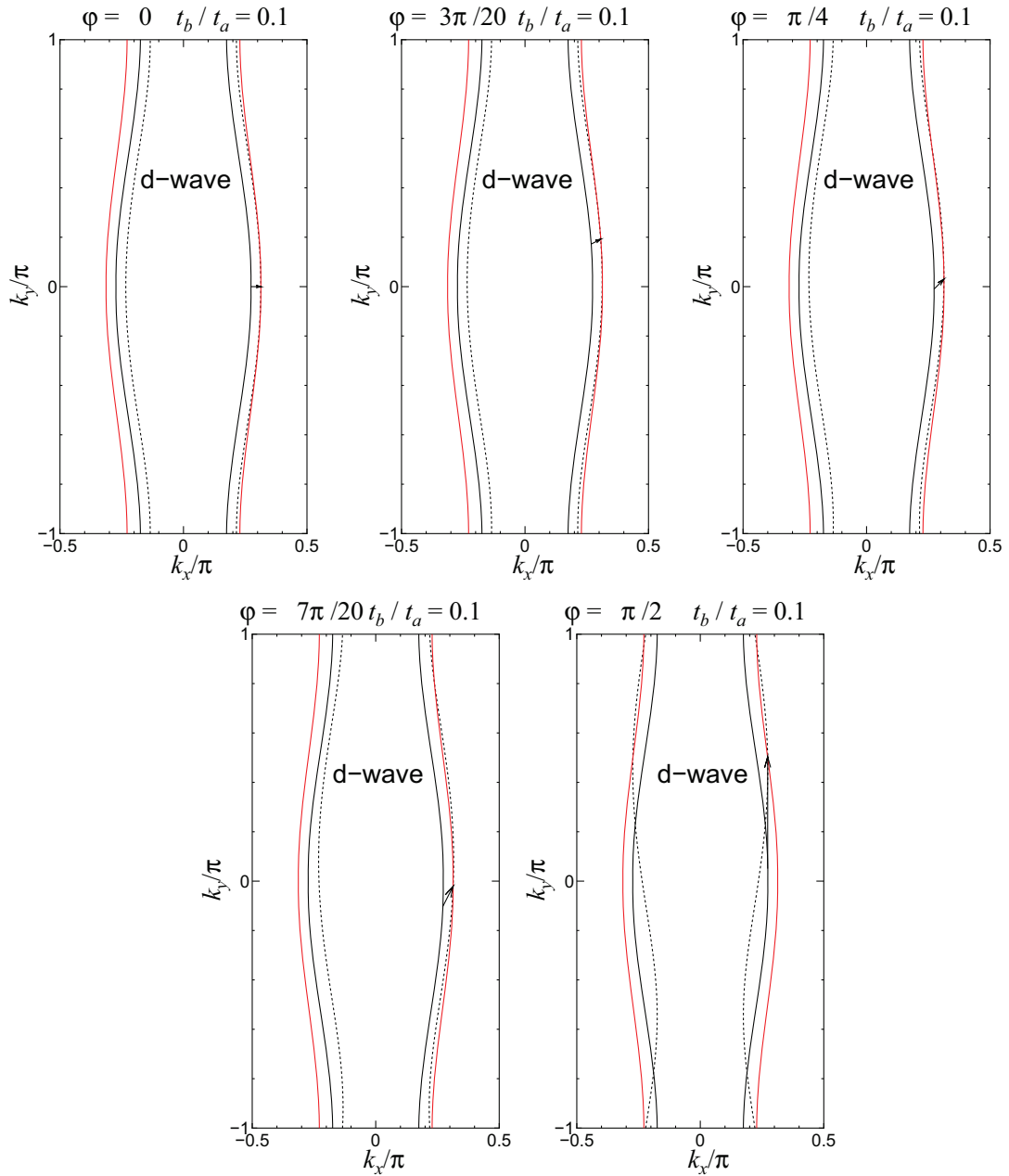
FIG. 19: Angle φ dependence of nesting condition for d-wave pairing and $t_b/t_a = 0.1$. See the caption of Fig. 18 for the meaning of the difference lines.

Figure 20 shows of the nesting condition for s-wave pairing and for angle $\varphi = 0, 97\pi/200, 49\pi/100$, and $\pi/2$. For large angles between $\boldsymbol{q}$ and $\boldsymbol{a}$, the curves of $H_{c2}(T)$ show the behavior of the typical of Q2D systems, and the nesting condition

is "touching on a line", similarly to $\varphi = 0$. The difference between the s-wave and d-wave states is due to the existance of the line nodes of the order parameter in the d-wave state. For $\varphi = 97\pi/200$, the nesting condition of touching on the right Fermi surface is favorable. For $\varphi \gtrsim 49\pi/100$, the nesting condition of touching on the left surface becomes more effective than that of touching on the right surface.
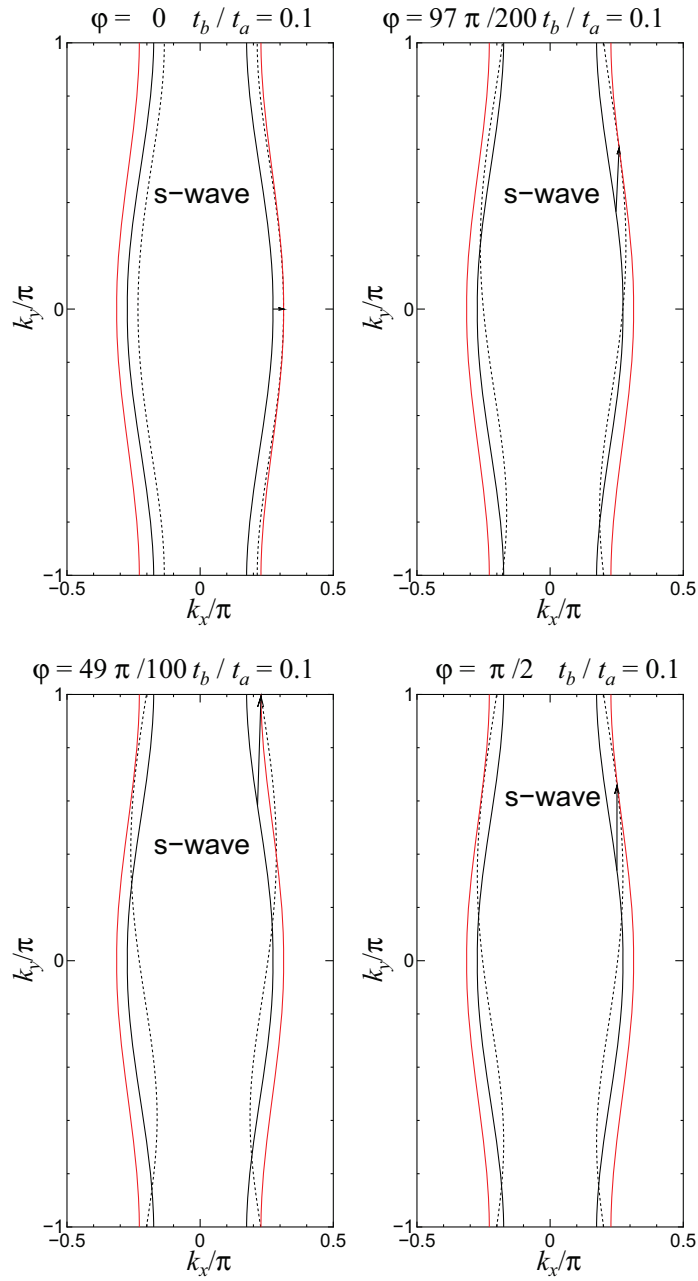
FIG. 20: Angle φ dependence of nesting condition for $t_b/t_a = 0.1$ with s-wave pairing. See the caption of Fig. 18 for the meaning of the difference lines.

6.3. Pauli paramagnetic limit

In this subsection, we present the numerical results for the Pauli paramagnetic limit. Figure 21 shows the temperature dependence of the Pauli paramagnetic limit for a 2D isotropic system. For s-wave pairing, $\mu_e H_{\mathrm{P}}/\Delta_{\mathrm{s0}} = 1/\sqrt{2}$ at $T = 0$. Although we cannot obtain the final result for the Q1D systems, similar results are expected by solving Eqs. (5.26) and (5.27). In Q1D system, $\mu_e H_{\mathrm{P}}/\Delta_{\mathrm{s0}}$ is equal to $1/\sqrt{2}$ at $T = 0$ for s-wave pairing as in the case of a 2D isotropic system. The Pauli paramagnetic limit for d-wave pairing is maximum value, $\mu_e H_{\mathrm{P}}/\Delta_{\mathrm{d0}} \approx 0.63$ (Fig. 22) at $T = 0$, when $t_b/t_a = 0.3$. The results show that the temperature dependence for d-wave is small.
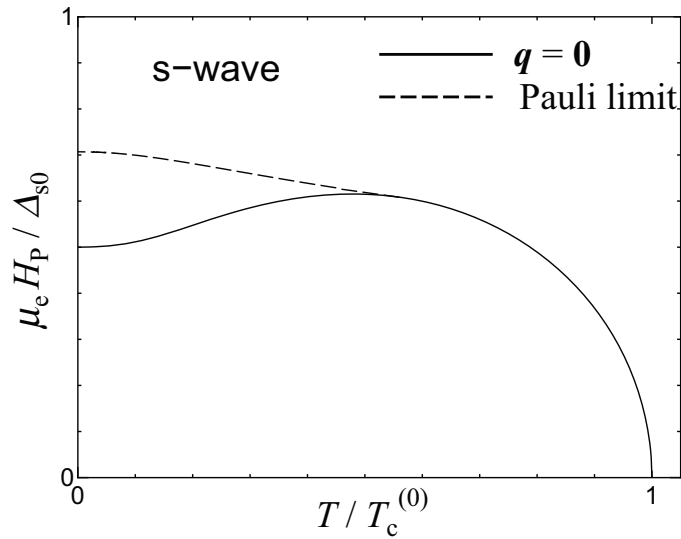
FIG. 21: Temperature dependence of the Pauli paramagnetic limit for s-wave pairing. The dashed curve shows the result for a 2D isotropic system. The solid curve is a upper critical field for $q = 0$.

Figure 22 presents the Pauli paramagnetic limit for d-wave pairing at $T = 0$. $\mu_e H_{\mathrm{P}}/\Delta_{\mathrm{d0}}$ slightly increases as t_b/t_a increases.
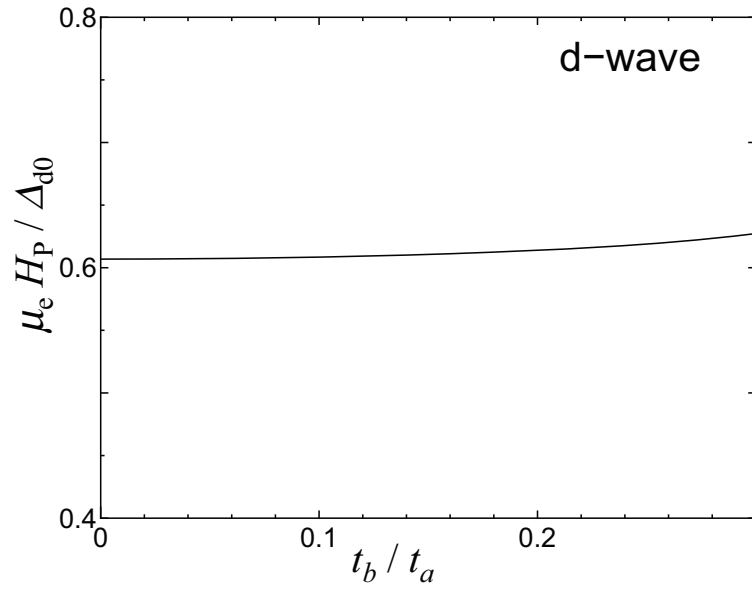
FIG. 22: t_b/t_a dependence of the Pauli paramagnetic limit for d-wave pairing.

7. SUMMARY AND DISCUSSION

The temperature dependence of the upper critical field $H_{c2}(T)$ has been calculated for various ratio of hopping integrals t_b/t_a and direction of $\boldsymbol{q}$ in Q1D s- and d-wave superconductivity. The qualitatively different behaviors of H_{c2} emerge depending on the values of these parameters.

In particular, the dimensional crossover from one dimension to two dimensions due to a temperature effect has been discovered. For $\boldsymbol{q} \parallel \boldsymbol{a}$ and $t_b/t_a \lesssim 0.1$, the behavior of H_{c2} looks like that of the 1D systems for $T^* \gtrsim T \gtrsim T_0$, while it is reduced to that of the Q2D systems for $T \lesssim T_0$. This dimensional crossover is found for both s- and d-wave pairings, although the upturn at low temperature for s-wave is weaker than that for d-wave. This crossover appears because the Fermi surfaces become diffuse owing to the thermal excitations at the energy scale $k_B T$. For $T^* \gtrsim T \gtrsim T_0$, the upper critical field behaves as if the Fermi-surface nesting is perfect as in the case of 1D. For $T \lesssim T_0$, the nesting condition is "touching on a line" as in the case of Q2D systems because the Fermi surface becomes sharp. Because T_0 is proportional to $t_b T_c^{(0)}/t_a$, T_0 is shift to high temperature side, as t_b/t_a increases. This dimensional crossover is quite different from the field-induced dimensional-crossover effect that has been studied so far by many authors [7, 45].

We have compared the present result with the experimental data in $(TMTSF)_2ClO_4$. When $\boldsymbol{H} \parallel \boldsymbol{a}$, $H_{c2}(T)$ shows a shoulder at low temperature. This behavior may relate to the present dimensional crossover. Detailed calculations of the temperature dependence upper critical fields that take into account both the Fermi-surface effect and the orbital effect remain for a future study. If the orbital effect is too strong, the behavior of $H_{c2}(T)$ would be simplified. If not, however, the second steep increase that indicates a d-wave FFLO state might be observed near $T = 0$.

When $\boldsymbol{q} \parallel \boldsymbol{a}$ and $0.2 \gtrsim t_b/t_a \gtrsim 0.15$, $H_{c2}(T)$ show a behavior typical of Q2D systems for s- and d-wave pairings, but a slight shoulder remains. For $t_b/t_a \gtrsim 0.2$, the slight shoulder disappears and $H_{c2}(T)$ qualitatively exhibits the typical behavior of the Q2D system in whole temperature range. This behavior may correspond to the monotonic behavior of $dH_{c2}(T)/dT$ in $(TMTSF)_2PF_6$ [22] if the pairing is spin

singlet. For $q \parallel a$, the behavior of $H_{c2}(T)$ below tricritical temperature T^* is summarized in Table III.

TABLE III: Behaviors of $H_{c2}(T)$ below the tricritical temperature T^*, when $q \parallel a$, i.e., $\varphi = 0$. The texts in the backets indicate the rate of increase.

t_b/t_a	d-wave		s-wave	
	$T \lesssim T_0$	$T_0 \lesssim T \lesssim T^*$	$T \lesssim T_0$	$T_0 \lesssim T \lesssim T^*$
small	Q2D (large)	1D	Q2D (small)	1D
large	Q2D	Q2D	Q2D	Q2D

It has been found that the upper critical field is maximum for $q \parallel a$ both for s-wave and d-wave pairings, independent of t_b/t_a. This direction of q was previously assumed but is not obvious *a priori* when the Fermi surface is warped.

$H_{c2}(T)$ for d-wave pairing exhibits the qualitatively different behaviors depending of the angles φ between q and a. When $\varphi \gtrsim \pi/4$, the upturn at low temperature disappears and $H_{c2}(T)$ curve is convex upward for d-wave pairing but the large shoulder remains. This behavior converges to a finite value $H_{c2}(0)$ with $dH_{c2}(0)/dT = 0$, i.e., corresponding to type (c) in Table II, as for 3D systems. For the optimum q, the Fermi surfaces cross along lines, but they do not touch on a line. This situation is irregular, as explained in Sect. 3, and it originates from the small curvature of the Q1D Fermi surface and the existence of the line nodes. On the other hand, for s-wave pairing, $H_{c2}(T)$ exhibits an upturn near $T = 0$, i.e., corresponding to type (b) in Table II, as for Q2D systems. Then, the Fermi surfaces touch on a line for all φ's. For $q \parallel b$, the $H_{c2}(T)$ is slightly higher than the Pauli paramagnetic limit and is not affected by the hopping integral parameters for both s- and d-wave pairings. For $t_b/t_a = 0.1$, the angle φ dependence of $H_{c2}(T)$ below tricritical temperature T^* is summarized in Table IV.

Now, we discuss the relation between the directions of the FFLO modulation vector q and the magnetic field H. For the discussion, let q_0 denote the optimum q in the absence of the orbital pair-breaking effect. This q_0 is determined by the

47

TABLE IV: Behaviors of $H_{c2}(T)$ below the tricritical temperature T^*, when $t_b/t_a = 0.1$. The texts in the backets indicate the rate of increase.

	d-wave		s-wave	
φ	$T \lesssim T_0$	$T_0 \lesssim T \lesssim T^*$	$T \lesssim T_0$	$T_0 \lesssim T \lesssim T^*$
small	Q2D (large)	1D	Q2D (small)	1D
large	3D	3D	Q2D	Q2D

Fermi-surface effect. There are two theoretical predictions for the relation of $\boldsymbol{q}$ and $\boldsymbol{H}$. When the orbital magnetic effect is strong, $\boldsymbol{q}$ is oriented to the direction of $\boldsymbol{H}$, as Gruenberg and Gunther proposed [51]. Since the degrees of the freedom perpendicular to $\boldsymbol{H}$ are used by the vortex state, the spatial modulation of the FFLO state can occur only in the direction of $\boldsymbol{H}$. The FFLO state is stabilized when $\boldsymbol{H} \parallel \boldsymbol{q}_0$ for the Fermi-surface effect. In contrast, when the Fermi-surface effect is much stronger than the orbital effect, $\boldsymbol{q}$ is locked in the direction of $\boldsymbol{q}_0$, independent of the magnetic field direction [41, 52], where the component of $\boldsymbol{q}$ perpendicular to $\boldsymbol{H}$ is realized by the Abrikosov functions with higher Landau level indexes.

In the experiment, the magnetic-field angle-dependence in H_{c2} has been observed. The experimental H_{c2} for the magnetic field along $\boldsymbol{b}'$-axis is larger than that along $\boldsymbol{a}$-axis. The present theoretical result that H_{c2} is the highest for $\boldsymbol{q} \parallel \boldsymbol{a}$ might appear to be inconsistent with the experimental result. However, since the orbital pair–breaking effect is weakest for $\boldsymbol{H} \perp \boldsymbol{q}$ according to the study by Croitoru et al., the theoretical result is consistent with the experimental result, if the direction of $\boldsymbol{q}$ is locked in the direction of $\boldsymbol{q}_0$.

The Pauli paramagnetic limit for s-wave pairing $\mu_e H_{\mathrm{P}}/\Delta_{\mathrm{s}0} = 1/\sqrt{2}$ at $T = 0$, independently t_b/t_a. That for d-wave pairing is maximum value, $\mu_e H_{\mathrm{P}}/\Delta_{\mathrm{d}0} \approx 0.63$ at $T = 0$, when $t_b/t_a = 0.3$.

In conclusion, Q1D s-wave and d-wave superconductors with various values of t_b/t_a and φ show qualitatively different behaviors of $H_{c2}(T)$, including hybrid behaviors of types (a) through (c). For $t_b/t_a \lesssim 0.1$ and $\varphi \lesssim 3\pi/20$, a novel dimen-

sional crossover from one dimension to two dimensions has been uncovered, which may be related to the non monotonic behavior of the upper critical field for $\boldsymbol{H} \parallel \boldsymbol{a}$ in $(TMTSF)_2ClO_4$. When $\boldsymbol{q}$ is parallel to the most conducting chain, $H_{c2}(T)$ is maximum for both s-wave and d-wave pairings. If the Fermi-surface effect is too strong, since $\boldsymbol{q}$ is oriented to the direction of $\boldsymbol{q}_0$, the theoretical angular dependence is consistent with the experimental date.

Acknowledgments

References

[1] P. Fulde and R. A. Ferrell, Phys. Rev. **135**, A550 (1964).

[2] A. I. Larkin and Yu. N. Ovchinnikov, Zh. Eksp. Teor. Fiz. **47**, 1136 (1964); translation: Sov. Phys. JETP, **20**, 762 (1965).

[3] R. Casalbuoni and G. Nardulli, Rev. Mod. Phys. **76**, 263 (2004).

[4] Y. Matsuda and H. Shimahara, J. Phys. Soc. Jpn. **76**, 051005 (2007).

[5] H. Shimahara, in *The Physics of Organic Superconductors and Conductors*, ed. A.G. Lebed (Springer, Berlin, 2008), p. 687.

[6] T. Ishiguro, K. Yamaji, and G. Saito, *Organic Superconductors* (Springer, Berlin, 1998), 2nd ed.

[7] N. Dupuis, Phys. Rev. B **51**, 9074 (1995); N. Dupuis, G. Montambaux, and C. A. R. Sá de Melo, Phys. Rev. Lett. **70**, 2613 (1993); N. Dupuis and G. Montambaux, Phys. Rev. B **49**, 8993 (1994).

[8] H. Shimahara, Phys. Rev. B **50**, 12760 (1994).

[9] H. Shimahara, J. Phys. Soc. Jpn. **66**, 541 (1997).

[10] H. Shimahara, J. Phys. Soc. Jpn. **68**, 3069 (1999); J. Supercond. **12**, 469 (1999).

[11] H. Shimahara and K. Moriwake, J. Phys. Soc. Jpn. **71**, 1234 (2002).

[12] J. Singleton, J. A. Symington, M.-S. Nam, A. Ardavan, M. Kurmoo, and P. Day, J. Phys. Condens. Matter **12**, L641 (2000).

[13] J. A. Symington, J. Singleton, M.-S. Nam, A. Ardavan, M. Kurmoo, and P. Day, Physica B **294–295**, 418 (2001).

[14] R. Lortz, Y. Wang, A. Demuer, P. H. M. Böttger, B. Bergk, G. Zwicknagl, Y. Nakazawa, and J. Wosnitza, Phys. Rev. Lett. **99**, 187002 (2007).

[15] J. A. Wright, E. Green, P. Kuhns, A. Reyes, J. Brooks, J. Schlueter, R. Kato, H. Yamamoto, M. Kobayashi, and S. E. Brown, Phys. Rev. Lett. **107**, 087002 (2011).

[16] S. Manalo and U. Klein, J. Phys. Condens. Matter **12**, L471 (2000).

[17] K. Maki and H. Won, Physica (Amsterdam) **322B**, 315 (2002).

[18] S. Uji, K. Kodama, K. Sugii, T. Terashima, Y. Takahide, N. Kurita, S. Tsuchiya, M.

Kimata, A. Kobayashi, B. Zhou, and H. Kobayashi, Phys. Rev. B **85**, 174530 (2012).

[19] M. Houzet, A. Buzdin, L. Bulaevskii, and M. Maley, Phys. Rev. Lett. **88**, 227001 (2002).

[20] H. Shimahara, J. Phys. Soc. Jpn. **71**, 1644 (2002).

[21] M.A. Tanatar, T. Ishiguro, H. Tanaka, and H. Kobayashi, Phys. Rev. B **66**, 134503 (2002).

[22] I. J. Lee, M. J. Naughton, G. M. Danner, and P. M. Chaikin, Phys. Rev. Lett. **78**, 3555 (1997).

[23] I. J. Lee, S. E. Brown, W. G. Clark, M. J. Strouse, M. J. Naughton, W. Kang, and P. M. Chaikin, Phys. Rev. Lett. **88**, 017004 (2001).

[24] J.I. Oh and M.J. Naughton, Phys. Rev. Lett. **92**, 067001 (2004).

[25] S. Yonezawa, S. Kusaba, Y. Maeno, P. Auban-Senzier, C. Pasquier, K. Bechgaard, and D. Jerome, Phys. Rev. Lett. **100**, 117002 (2008).

[26] S. Yonezawa, S. Kusaba, Y. Maeno, P. Auban-Senzier, C. Pasquier, and D. Jerome, J. Phys. Soc. Jpn. **77**, 054712 (2008).

[27] M. Takigawa, H. Yasuoka, and G. Saito, J. Phys. Soc. Jpn. **56**, 873 (1987).

[28] A.G. Lebed, Phys. Rev. Lett. **107**, 087004 (2011).

[29] M.D. Croitoru, M. Houzet, and A.I. Buzdin, Phys. Rev. Lett. **108**, 207005 (2012).

[30] M. Miyazaki, K. Kishigi, and Y. Hasegawa, J. Phys. Soc. Jpn. **68**, 3794 (1999).

[31] A.G. Lebed and S. Wu, Phys. Rev. B **82**, 172504 (2010).

[32] H. Aizawa, K. Kuroki, T. Yokoyama, and Y. Tanaka, Phys. Rev. Lett. **102**, 016403 (2009).

[33] Y. Fuseya, C. Bourbonnais, and K. Miyake, Eur. Phys. Lett. **100**, 57008 (2012).

[34] A. G. Lebed JETP Lett. **94**, 689 (2011).

[35] D. L. Pevelen, J. Gaultier, Y. Barrans, D. Chasseau, F. Castet, and L. Ducasse, Eur. Phys. J. B **19**, 363 (2001).

[36] Y. Nagai, H. Nakamura, and M. Machida, Phys. Rev. B **83**, 104523 (2011).

[37] S. Haddad, N. Belmechri, S. Charfi-Kaddour, and M. Heritier, Phys. Rev. B **78**, 075104 (2008).

[38] Y. Hasegawa and M. Miyazaki, J. Phys. Soc. Jpn. **65**, 1028 (1996).

[39] N. Belmechri, G. Abramovici, and M. Heritier, Europhys. Lett. **82**, 47009 (2008).

[40] N. Miyawaki and H. Shimahara, J. Phys. Soc. Jpn. **83**, 024703 (2014).

[41] H. Shimahara and D. Rainer, J. Phys. Soc. Jpn. **66**, 3591 (1997).

[42] A. M. Clogston, Phys. Rev. Lett. **9**, 266 (1962); B.S. Chandrasekhar, Appl. Phys. Lett. **1**, 7 (1962).

[43] H. Burkhardt and D. Rainer, Ann. Physik **3**, 181 (1994).

[44] L.N. Bulaevskii, Zh. Eksp. Teor. Fiz. **65**, 1278 (1973); translation: Sov. Phys. JETP **38**, 634 (1974).

[45] A. G. Lebed, Pis'ma Zh. Eksp. Teor. Fiz. **44**, 89 (1986); translation: JETP Lett. **44**, 114 (1986).

[46] H. Shimahara, J. Phys. Soc. Jpn. **67**, 736 (1998).

[47] K. Machida and H. Nakanishi, Phys. Rev. B **30**, 122 (1984).

[48] Y. Suzumura and K. Ishino, Prog. Theor. Phys. **70**, 654 (1983).

[49] A. I. Buzdin and V. V. Tugushev, Zh. Eksp. Teor. Fiz. **85**, 73 (1983); translation: Sov. Phys. JETP **58**, 428 (1983).

[50] The dimensional crossover effect examined here is different from that concerning the orbital magnetic effect examined in Refs. [7] and [45].

[51] L. W. Gruenberg and L. Gunther, Phys. Rev. Lett. **16**, 996 (1966).

[52] H. Shimahara, Phys. Rev. B **80**, 214512 (2009).

[53] In the weak coupling theory, the pure paramagnetic limit is estimated to be $H_{\mathrm{P}} = 2.3$ T for $t_b/t_a = 0.1$, $g = 2$, and d-wave pairing, which is smaller than $1.86\,\mathrm{T/K} \times T_{\mathrm{c}}^{(0)}[\mathrm{K}] \approx 2.7$ T for isotropic pairing, if $T_{\mathrm{c}}^{(0)} = 1.45$ K is assumed [9].